# Mutation in the Bone Morphogenetic Protein signaling pathway sensitize zebrafish and human to ethanol-induced jaw malformations

John R. Klem[1], Tae-Hwi Schwantes-An[2], Marco Abreu[2], Michael Suttie[3,4], Raeden Gray[1], Hieu Vo[1], Grace Conley[1], Tatiana M. Foroud[2], Leah Wetherill[2] , CIFASD, and C. Ben Lovely[1*].

[1]University of Louisville School of Medicine, Department of Biochemistry and Molecular Genetics, Alcohol Research Center, Louisville, KY

[2]Department of Medical and Molecular Genetics, Indiana University School of Medicine, Indianapolis, IN

[3]Nuffield Department of Women's and Reproductive Health, University of Oxford, Oxford, United Kingdom.

[4]Big Data Institute, University of Oxford, Oxford, United Kingdom.

* correspondence to: ben.lovely@louisville.edu

## Abstract

**Background:** Fetal Alcohol Spectrum Disorders (FASD) describe a continuum of ethanol-induced developmental defects including commonly observed craniofacial malformations. While ethanol-sensitive genetic mutations are a major contributor to facial malformations, the impacted cellular mechanisms underlying these facial anomalies remain unknown. The Bone Morphogenetic Protein (Bmp) signaling pathway is a key regulator of epithelial morphogenesis driving facial development, providing a possible ethanol-sensitive mechanism to malformations to the facial skeleton.

**Methods:** Using zebrafish, we tested several mutants for Bmp pathway components for ethanol-induced facial malformations. Mutant embryos were exposed to ethanol in the media from 10-18 hours post-fertilization (hpf). Exposed zebrafish were fixed at 36 hpf to analyze anterior pharyngeal endoderm size and shape by immunofluorescence or at 5 days post-fertilization (dpf) to quantitatively examine shape of the facial skeleton stained with Alcian Blue/Alizarin Red staining. Integrating human genetic data, we screened for Bmp-ethanol associations in jaw volume of ethanol-exposed children.

**Results:** We found that mutations in the Bmp pathway sensitize zebrafish embryos to ethanol-induced malformations to anterior pharyngeal endoderm shape, leading to altered expression of *fgf8a* in the oral ectoderm. These changes correlate with shape changes in the viscerocranium, suggesting that ethanol-induced malformations of the anterior pharyngeal endoderm lead to facial malformations. Variants in the Bmp receptor gene, *BMPR1B* were associated with ethanol-related differences in jaw volume in humans.

**Conclusions:** For the first time, we show that ethanol exposure disrupts proper morphogenesis of, and tissue interactions between, the facial epithelia. These shape changes in the anterior pharyngeal endoderm-oral ectoderm-signaling axis during early zebrafish development mirror the overall shape changes observed in the viscerocranium and were predictive for Bmp-ethanol associations in jaw development in human. Collectively, our work provides a mechanistic paradigm linking the impact of ethanol to the epithelial cell behaviors that underlie facial defects in FASD.

## Keywords

Fetal Alcohol Spectrum Disorders, Zebrafish, Alcohol, Genetics, FASD, Endoderm, Jaw development.

## Introduction

Ethanol is the most common environmental risk factor for congenital anomalies, with Fetal Alcohol Spectrum Disorders (FASD) describing all ethanol-induced birth defects. Highly variable, multiple phenotypes present with FASD include structural malformations to the brain and face (Lovely, 2020). At the most severe end of the FASD spectrum is Fetal Alcohol Syndrome (FAS), which frequently presents as craniofacial defects including jaw hypoplasia (Basart et al., 2018; Blanck-Lubarsch et al., 2020; Naidoo et al., 2005). However, increasing data indicates that prenatal alcohol exposure (PAE) results in craniofacial defects in the absence of a diagnosis of FAS (Muggli et al., 2017; Suttie et al., 2013). Multiple factors contribute to the impact of PAE, in particular genetic predisposition (Lovely, 2020). To date, several ethanol sensitizing alleles in *Shh, pdgfra, foxi, vangl2, Aldh2, Fancd2, and ADH1C* have been linked with increased cell death, holoprosencephaly, oral clefting, disruption to axonal projections and broad neural and eye defects (Boyles et al., 2010; Hong and Krauss, 2012; Langevin et al., 2011; McCarthy et al., 2013; Swartz et al., 2014; Zhang et al., 2013). And yet, while we have gained a greater understanding of the genetic components contributing to risk for FASD, we lack mechanistic insights into ethanol-sensitive gene function and associated cellular mechanisms during development that underlie FASD (Lovely, 2020).

Increasing evidence from several vertebrates including human shows that genetic factors modulate developmental ethanol sensitivity (reviewed in (Eberhart and Parnell, 2016; Lovely, 2020)). Studying FASD in humans is challenging due to the complex interplay of genetic background with ethanol timing and dosage. Genetically tractable model organisms, such as zebrafish, have been essential in improving our understanding of the genetic loci behind the variability in FASD (Fernandes and Lovely, 2021). The zebrafish is well-suited for studying ethanol-sensitizing genetics because of its genetic tractability, high fecundity, external fertilization, embryo transparency, and rapid development (Everson et al., 2022; McCarthy et al., 2013; Swartz et al., 2020, 2014). We have previously used both a candidate-based and an unseparated un-biased forward-genetic screen-based approach to identify ethanol-sensitive mutations (McCarthy et al., 2013; Swartz et al., 2020, 2014) and these approaches have proven successful in predicting human gene-ethanol interactions (McCarthy et al., 2013). However, despite the increasing number of identified ethanol-sensitive loci, we lack a conceptual and mechanistic understanding of how

these gene-ethanol interactions affect the diverse cell types and cellular behaviors underlying craniofacial development.

Previous work has established that both the genetic pathways required in, and the cellular events for, development of the craniofacial skeleton are deeply conserved between zebrafish and mammals (Clouthier and Schilling, 2004; Depew et al., 2002; Trainor et al., 2003). Cranial neural crest cells (CNCC) give rise to the majority of the craniofacial skeleton and migrate from the dorsal neural tube to populate progenitor structures called the pharyngeal arches (Cordero et al., 2011; Knight and Schilling, 2006; Mork and Crump, 2015; Trainor et al., 2003). Concurrent with cranial neural crest cell migration, the pharyngeal endoderm undergoes its own cellular rearrangements and tissue movements to form a midline epithelial sheet with lateral protrusions called “pouches”. Proper morphogenesis of the pharyngeal endoderm is critical for craniofacial development, in particular of the jaw (Arnold, 2006; Balczerski et al., 2012; Chong Pyo Choe and Crump, 2015; Couly et al., 2002; Crump, 2004a; David et al., 2002; Haworth et al., 2004, 2007; Liu et al., 2005; Lovely et al., 2016). Work in zebrafish has shown that several genetic pathways regulate endodermal morphogenesis (Choe et al., 2013; Choe and Crump, 2014; Crump, 2004b; David et al., 2002; Hu et al., 2018; Li et al., 2019; Lovely et al., 2016). One such pathway is the Bone Morphogenetic Protein (Bmp) signaling pathway. Comprised of over 60 pathway components with different spatio-temporal expression and activity, active Bmp signaling initiates with heterodimer ligands binding to a complex of two type I and two type II transmembrane receptors that regulate downstream target genes through phosphorylation of Smad proteins (Kondo, 2007; Little and Mullins, 2009). Two major interacting ligands of the pathway are *bmp2b* and *bmp4*, both of which have a higher binding affinity type I Bmp receptors, such as *bmpr1bb* over type II receptors (Little and Mullins, 2009; Tajer et al., 2021). We have previously shown that Bmp signaling is required in the endoderm to regulate a Fibroblast Growth Factor (Fgf) signaling response in the forming pouches (Lovely et al., 2016). We previously blocked Bmp signaling with the small chemical inhibitor dorsomorphin from 10-18 hpf, which disrupted morphogenesis of both pouches and the anterior pharyngeal endoderm, the area of endoderm anterior to the first pouch, resulting in craniofacial malformations (Lovely et al., 2016). These observations showed that functional Bmp signaling was indispensable to establish proper endoderm morphology as necessary for proper craniofacial formation.

Bmp signaling is a complex pathway that is essential for craniofacial morphogenesis, suggesting that it is potentially ethanol-sensitive. Here, we tested the ethanol sensitivity of multiple mutants in the Bmp pathway. We show that mutants either hemizygous or homozygous for the Bmp ligand genes *bmp2b* and *bmp4* and the receptor gene *bmpr1bb* (defined as Bmp mutants for simplicity) predispose zebrafish embryos to distinct ethanol-induced craniofacial shape changes, particularly jaw malformations. We show that ethanol-induced disruptions to anterior pharyngeal endoderm shape, which mirror changes in facial shapes, alter the expression domain of the oral ectoderm marker *fgf8a* as associated with jaw malformations. Genetic analysis shows that *BMPR1B* associates with jaw deformations in children with ethanol exposure that mirror our zebrafish data, underlining the predictive strength of our zebrafish studies. Collectively, our data links perturbations in Bmp signaling to ethanol susceptibility during craniofacial development in zebrafish and humans, establishing mechanistic concepts in gene-ethanol interactions for future studies in FASD.

## Materials and Methods

### Zebrafish (*Danio rerio*) care and use

All zebrafish were raised and cared for using established IACUC protocols approved by the University of Louisville (Westerfield, 2007). Adult fish were maintained at 28.5°C with a 14 / 10-hour light / dark cycle. The *bmp2b*$^{tc300a}$ (Mullins et al., 1996), *bmp4*$^{st72}$ (Stickney et al., 2007), *bmpr1bb*$^{sw40}$ (Neumann et al., 2011) and *smad5*$^{b1100}$ (Swartz, 2011) and *sox17:EGFP*$^{s870}$ (Chung and Stainier, 2008a) zebrafish lines were previously described.

### Zebrafish staging and ethanol treatment

Eggs were collected and embryos were morphologically staged (Westerfield, 2007), sorted into sample groups of 100 and reared at 28.5°C to desired developmental time points. All groups were incubated in embryo media (EM). At 10 hpf, EM was changed to either fresh EM or EM containing 1% ethanol (v/v). At 18 hpf, EM containing ethanol was washed out with 3 fresh changes of EM.

### Hybridization chain reaction (HCR) and immunofluorescence

Embryos were collected at 36 hpf, dechorionated and fixed in 4% paraformaldehyde/PBS at 4°C. HCR protocol was previously described (Ibarra-García-Padilla et al., 2021). HCR amplifiers and buffers were

acquired from Molecular Instruments (Molecular Instruments). Probes against *fgf8a* were designed as previously described (Kuehn et al., 2022). Immunofluorescence was performed as previously described (Lovely et al., 2016). Primary antibody was anti-GFP (sc-9996, Santa Cruz), secondary antibody was Alexa Fluor 488 (A10042, Invitrogen).

**Imaging & analysis of anterior pharyngeal endoderm shape**

Confocal images were taken using an Olympus FV1000 microscope and measured in FIJI (Schindelin et al., 2012). The anterior pharyngeal endoderm was defined as the medial endoderm anterior to the first pouch. General head area was defined as the product of the width and length of the embryo anterior to the first pouch.

**Cartilage and Bone staining**

Zebrafish larva fixed at 5 dpf were stained with alcian blue for cartilage and alizarin red for bone (Walker and Kimmel, 2007). Whole mount, ventral view, brightfield images of the viscerocranium were taken on an Olympus BX53 compound microscope.

**Morphometric analyses**

Morphometric analysis of alcian/alizarin-stained larva was performed in TpsDig2 (https://sbmorphomectrics.org) and MorphoJ (Klingenberg, 2011). Landmarks were placed on the following joints, Meckel's cartilage midline joint, the joints between Meckels' and the palatoquadrate, the palatoquadrate and ceratohyal and at the end of the hyomandibular cartilages. Linear measures were analyzed using TpsDig2. Principle component analysis (PCA), Procrustes ANOVA and wireframe graphs of facial variation were generated using MorphoJ.

**Statistical analyses**

Meckel's cartilage area was analyzed with a one-way ANOVA with a Tukey's Multiple Comparisons Test and linear measures/angles of both the anterior endoderm and Alcian/alizarin-stained viscerocranium were analyzed with a two-way ANOVA (type III) with a Tukey's Multiple Comparisons Test in Graphpad Prism 9.5.1 (Graphpad Software Inc., La Jolla, CA).

**Human Study**

Human participants were recruited as part of the Collaborative Initiative on FASD (CIFASD) from (2007-2017) from sites in Atlanta, GA, Los Angeles, CA, Minneapolis, MN, and San Diego, CA (Mattson et al., 2010a, 2010b). Institutional Review Board approval was obtained at each site. All participants and/or their

parents/legal guardians provided written informed consent. Children (aged 5-18 years) who experienced heavy (>4 drinks/occasion at least weekly or >13 drinks/week) prenatal alcohol exposure (PAE) with or without a diagnosis of FAS were classified as PAE, and those who were exposed to minimal (<1 drink/week or <2 drinks/occasion) or no PAE were classified as no PAE (Mattson et al., 2010a, 2010b). 3D images were obtained on most participants at the time of the dysmorphology exam using static stereophotogrammetric camera systems capable of capturing a 180-degree image of facial surface geometry. Each image was annotated with a sparse set of 20 reliable anthropometric landmarks (Supplement Fig. 1A). We performed a Procrustes alignment on the landmarks of each face, aligning them to a template face using a similarity transform. The transform was applied to each 3D surface to normalize size to a uniform scale. To evaluate micrognathia, we computed mandible volume, which was outlined and validated against CT images in (Basart et al., 2018). This technique estimated the volume of a trapezoid formed by four specific points on the size-normalized face: the left and right lower otobasion inferius (lowest points of the ears), gnathion (tip of the mandible), and lower lip vermillion center (Supplement Fig. 1B).

Genome-wide association study (GWAS) data were genotyped on the OmniExpress genome array (Illumina, San Diego CA) and on the Multi-Ethnic Genotyping Array at the Johns Hopkins Genetic Resources Core Facility (Baltimore, MD; Dou et al., 2018). Following a previously published GWAS cleaning pipeline (Schwantes- An et al., 2021), the two datasets were cleaned for sample and variant call rates, Hardy-Weinberg Equilibrium (HWE), sample identity using genetic (calculated from single nucleotide polymorphisms [SNPs] on X and Y chromosomes) and self-reported sex, sample relatedness, and genetic ancestry. The two cleaned datasets were imputed separately using Michigan Imputation Server (Das et al., 2016) to 1000-Genomes Phase 3, b37 reference panel (Fairley et al., 2020) then combined. The final dataset consisted of 4,000,362 genotyped and imputed SNPs with minor allele frequency (MAF) ≥ 0.01, genotype rate ≥0.99, and Hardy-Weinberg equilibrium p≥0.000001. Principal components analysis (PCA) was performed using SNPRelate (Zheng et al., 2012) with genotype data from autosomes. Individuals in the 1000-Genomes database (Fairley et al., 2020) were included as reference samples for clustering individuals based on genetic ancestry similarities. Individuals were grouped with European Ancestry (EA,

n=222), African Ancestry (AA, n=103) or other (n=44) ancestry samples from 1000 Genomes Project using the first three principal components. Only EA and AA individuals were included in our analyses.

Analyses were performed separately in the EA and AA groups using R (version 4.2.0; R Foundation for Statistical Computing; http://cran.r-project.org/) and PLINK v2.00a3 64-bit (8 Jun 2021). Association of SNP genotype with mandible volume was assessed using an additive generalized linear model with sex, age at time of 3D image, the first 10 genetic principal components, PAE and genotype by PAE interaction. As the effect of interest was the association of genotype with mandible volume with and without the presence of PAE, the p-value for the genotype by PAE interaction is reported. Variants within 25 kilobase pairs of the three genes of interest (*BMP2, BMP4, BMPR1B*) were evaluated in the EA group to identify significant SNPs ($p<0.05$). To further explore the genotype by PAE interaction, we employed a non-parametric Wilcoxon test (SAS v 9.4) to compare mandible volume in individuals with PAE to those without PAE stratified by genotype, and to compare mandible volume by genotype groups stratified by PAE. All analyses were performed in the EA and AA samples separately.

## Results

### Mutations in multiple components of the Bmp pathway sensitize embryos to ethanol-induced viscerocranial malformations

Our previous work showed that Bmp signaling is required in the endoderm from 10-18 hpf (Lovely et al., 2016). We showed that the genes *bmp2b* and *bmp4* encoding Bmp ligands are expressed adjacent to the development endoderm during this time window, making these gene ideal targets for ethanol-sensitivity testing (Lovely et al., 2016). Both of Bmp2b and Bmp4 have a higher binding affinity type I Bmp receptors over type II (Little and Mullins, 2009; Tajer et al., 2021). As such, we also tested the receptor mutant *bmpr1bb* (Neumann et al., 2011). We hypothesized that mutations in these Bmp signaling pathway components would sensitize embryos to ethanol-induced craniofacial malformations.

To test these Bmp mutants, we exposed embryos to a sub-phenotypic dose of 1% ethanol (v/v) from 10-18 hpf, the same window when Bmp signaling is required for endoderm morphogenesis and jaw development (Lovely et al., 2016). We selected 1% ethanol (v/v) as it is the highest dose that does not

cause craniofacial defects in wild type embryos, while higher doses, 1.25% and up, have been shown to impact facial development (Bilotta et al., 2004; Everson et al., 2022, 2020; McCarthy et al., 2013; Swartz et al., 2014; Zhang et al., 2014). This dose equilibrates within 5 minutes of exposure to an average ethanol tissue concentration of 50 mM (approximately 30% of the media) (Flentke et al., 2014; Lovely et al., 2014; Reimers et al., 2004; Zhang et al., 2013). Importantly, this embryonic ethanol concentration is roughly equivalent to a human BAC of 0.23; while a binge dose, is physiologically relevant to FASD and humans are easily capable of surpassing this amount (Canfield et al., 2019; Ethen et al., 2009; Jones, 2008; Maier, 2001; Whaley et al., 2019).

Using this exposure paradigm, we found that mutations in our chosen Bmp mutants sensitize developing zebrafish to a range of ethanol-induced developmental defects, including cardiac edema (data not shown), small eyes and, for this work, jaw malformations (Fig. 1A-H). While *bmp2b*$^{-/-}$ embryos do not develop past 16 hpf (Nguyen et al., 1998), *bmp2b*$^{+/-}$, *bmp4*$^{-/-}$, or *bmpr1bb*$^{-/-}$ larvae undergo normal craniofacial development and are indistinguishable from their wild type siblings (Fig. 1A-D). However, when exposed to ethanol using our conditions, the Bmp mutants develop a variable range of jaw defects from malformations to outright absence of the jaw (Fig. 1 E-F). Jaw malformations were more common in ethanol-treated Bmp mutants than absent jaw, with 15.9% vs 4.6% in *bmp2b*$^{+/-}$, 37.8% vs 6.13% in *bmp4*$^{-/-}$, and 29.1% vs 2.7% in *bmpr1bb*$^{-/-}$, with variation between experimental groups (Table 1). Our quantifications also demonstrated that while wild type siblings never displayed sensitivity to ethanol, heterozygous *bmp4*$^{+/-}$ and *bmpr1bb*$^{+/-}$ larva were ethanol sensitive with incomplete penetrance (Table 1). These results reveal that viscerocranial malformations, in particular jaw absence only occur in ethanol-treated animals with Bmp pathway mutations and not in either Bmp mutant or ethanol treatment alone.

**Ethanol alters overall shape of the viscerocranium in Bmp mutants**

Micrognathia is a hallmark of ethanol exposure in human, though recent data has shown greater variation in facial shape in FASD (Blanck-Lubarsch et al., 2020; Suttie et al., 2013). To understand the impact of ethanol on viscerocranial shape and size, we undertook as series of quantitative measures to directly assess facial shape changes in zebrafish. To quantify micrognathia-like reductions in jaw size observed in FASD, we dissected and measured the size of the Meckel's cartilages from untreated *bmp2b*$^{+/-}$ and

ethanol-treated *bmp2b*$^{+/+}$ and *bmp2b*$^{+/-}$ larva. Ethanol-treated *bmp2b*$^{+/-}$ larva displayed a significant reduction in jaw size compared to untreated *bmp2b*$^{+/-}$ and ethanol-treated *bmp2b*$^{+/+}$ larva (Fig. 1I, one-way ANOVA, F=36.85, p<.0001). Beyond jaw defects, we observed malformations in additional viscerocranial cartilage elements, in particular an increase of the angle between the ceratohyal (Ch) elements (Fig. 1B-D compared to F-H). To expand our assessment of Bmp-ethanol interactions on facial shape, we performed morphometric analysis on untreated and ethanol-treated *bmp4*$^{+/+}$ and *bmp4*$^{-/-}$ larva. We analyzed *bmp4* larva as they showed the greatest variation due to ethanol treatment. (Table 1). We determined facial shape by labeling each joint in the viscerocranium (Fig. 2, Alcian Blue-stained image, untreated *bmp4*$^{+/+}$ (n=61) and *bmp4*$^{-/-}$ (n=54) larva; ethanol-treated *bmp4*$^{+/+}$ (n=58) and *bmp4*$^{-/-}$ (n=66) larva). Principle component analysis (PCA) of facial shape revealed that PC1 represented over 50% of facial variation as a shortening and widening of the viscerocranium, as well as a flattening of the angles of several cartilage elements (Fig. 2, Principal component 1). PC2 represented nearly 20% of the variation in facial shape, affecting width of the midface (Fig. 2, Principal component 2). Our dataset shows that the greatest amount of variation occurred in ethanol-treated *bmp4*$^{-/-}$ larva, while the smallest variation occurred in wild type, *bmp4*$^{+/+}$ larva (Fig. 2, magenta dashed vs black dashed 95% confidence ellipses). Ethanol-treated *bmp4*$^{+/+}$ and untreated *bmp4*$^{-/-}$ larva displayed similar increases in variation compared to untreated *bmp4*$^{+/+}$ larva, but less than ethanol-treated *bmp4*$^{-/-}$ larva. The mean of each group, displayed as a solid ellipse centered in the 95% confidence ellipse, shows little overlap between the groups (Fig. 2). Procrustes ANOVA analysis showed that these shape changes were significant (F=10.37, p<.0001). Combined, our morphometric data set shows that ethanol-treated *bmp4*$^{-/-}$ larva displayed significant variation in facial shape; however, either ethanol or *bmp4*$^{-/-}$ alone also increase variation in viscerocranial shape compared to untreated *bmp4*$^{+/+}$ larva. We did not identify this variation in ethanol or *bmp4*$^{-/-}$ alone in our initial visual screens. Overall, this data shows that ethanol-treated Bmp mutants larvae have significant, quantifiable changes in facial size and shape compared that are not readily identified in visual screens for gross morphology.

To confirm the morphometric data, we performed linear measurements on the viscerocrania of the *bmp4* dataset. We measured the length between the midline joints of the Meckel's and ceratohyal cartilages and the width between the joints of the Meckel's and palatoquadrate cartilages and ceratohyal and

palatoquadrate cartilages (Fig. 3A). We further performed angle measures of the joints of the Meckel's and ceratohyal cartilages to analyze the flattening of the viscerocranium cartilage elements (Fig. 3E). Consistent with PC1 (Fig. 2), we observed a significant decrease in the length between the Meckel's and ceratohyal cartilages in ethanol-treated *bmp4*$^{-/-}$ larva compared to all other groups (Fig. 3B, Table 2). We also observed significant changes in facial width at both the Meckel's and palatoquadrate cartilages and ceratohyal and palatoquadrate cartilages (Fig. 3C and D, respectively, Table 2). In both measures, ethanol-treated *bmp4*$^{-/-}$ larva showed significant decreases in width at both the Meckel's and palatoquadrate cartilages and ceratohyal and palatoquadrate cartilages compared to untreated *bmp4*$^{+/+}$ larva and untreated *bmp4*$^{-/-}$ larva (Fig. 3C-D, Table 2). In contrast, untreated *bmp4*$^{-/-}$ larva showed an increase in viscerocranial width compared to all other groups; the measurements were significantly increased compared to ethanol-treated *bmp4*$^{+/+}$ and *bmp4*$^{-/-}$ larva (Fig. 3C-D, Table 2) and trending toward significance compared to untreated wild type embryos in Fig. 3C (Table 2) but not in Fig. 3D (Table 2). In angle measures of the Meckel's and ceratohyal cartilages, ethanol-treated *bmp4*$^{-/-}$ larva showed significant increases in cartilage angles (Fig. 3F-G, Table 2), consistent with the flattening of the viscerocranial cartilages observed initial screens (Fig. 1) and PC1 and PC2 of our morphometric analysis (Fig. 2). Overall, this data documents the impact the Bmp-ethanol interaction results in a smaller jaw, and shorter and wider viscerocranial shape, consistent with FASD in humans.

**Combinatorial loss of Bmp pathway components exacerbates ethanol-induced viscerocranial malformations**

While we consistently observed ethanol-induced viscerocranial shape changes in tested Bmp mutants that differed from wild type controls, both the penetrance and expressivity of these defects were highly variable (Figs. 1-3, Table 1). The Bmp pathway is a complex signaling pathway comprised of multiple components (Little and Mullins, 2009). These components can be partially redundant at different levels of the pathway (Li et al., 2011; Mu et al., 2021; Schille et al., 2016; Wise and Stock, 2010). Given this redundancy, we hypothesized that combinatorial loss of pathway components potentially increases both the penetrance and expressivity of ethanol-induced viscerocranial defects. Using a hypomorphic *smad5* allele that has a highly stereotyped phenotype of cartilage fusions and malformations and have been previously shown to be insensitive to ethanol exposure (McCarthy et al., 2013; Swartz et al., 2011), we generated double-

mutant *bmp4*$^{-/-}$;*smad5*$^{-/-}$ larvae (Fig. 4). We found that *bmp4*$^{-/-}$;*smad5*$^{-/-}$ larvae exhibit 100% penetrant, ethanol-induced viscerocranial malformations that are a) more severe than the stereotypical *smad5* phenotypes in untreated *bmp4*$^{-/-}$;*smad5*$^{-/-}$ larva and b) much more severe than any of the Bmp single mutants (Fig. 4D compared to B; compared to Fig. 1). We also observed a spectrum of phenotype severity in *bmp4*$^{+/-}$;*smad5*$^{-/-}$ larvae, in which one gene copy of *bmp4* remains wild-type: these phenotypes range from stereotypical *smad5* mutant phenotypes to phenotypes comparable to ethanol-treated double-homozygous *bmp4*$^{-/-}$;*smad5*$^{-/-}$ larvae (Supp. Fig. 1). In contrast, we observed no impact of ethanol on double-heterozygous *bmp4*$^{+/-}$;*smad5*$^{+/-}$ larvae (Supp. Table 1). These genetic interaction results indicate that the variation in *bmp*$^{+/-}$;*smad5*$^{-/-}$ larvae may be driven either by expression differences in other components of the Bmp pathway or additional yet identified ethanol-sensitive alleles. Ultimately, these data supports our previous observation in *bmp4*$^{-/-}$ larva that ethanol-induced phenotypes only occur in the combination of mutation and ethanol exposure, indicating that the interaction of BMP signaling with ethanol is synergistic during craniofacial development.

**Ethanol-treated Bmp mutants display malformations to the anterior pharyngeal endoderm and *fgf8a* expression in the oral ectoderm**

We have previously shown that zebrafish embryos treated with the Bmp signaling inhibitor compound Dorsomorphin from 10-18 hpf exhibit disrupted morphogenesis of the anterior pharyngeal endoderm (Lovely et al., 2016). Multiple studies have shown that disruptions to the anterior pharyngeal endoderm leads to jaw malformations (Balczerski et al., 2012; Chong Pyo Choe and Crump, 2015; Couly et al., 2002; Crump, 2004a; David et al., 2002; Haworth et al., 2004, 2007). To analyze anterior pharyngeal endoderm shape, we labeled the pharyngeal endoderm by crossing the *sox17:EGFP* transgene, which labels all endoderm with GFP (Chung and Stainier, 2008b), into the *bmp4*$^{-/-}$;*smad5*$^{-/-}$ background. Compared to wild type, ethanol-treated *bmp4*$^{-/-}$;*smad5*$^{-/-}$ larvae showed mild changes to overall endoderm shape (Fig. 5A-D). However, our more detailed examination showed that the shape of the anterior pharyngeal endoderm is altered in ethanol-treated *bmp4*$^{-/-}$;*smad5*$^{-/-}$ larvae (Fig. 5A'-D'). To quantify these changes in anterior pharyngeal endoderm shape, we measured width at the first pouch (AE width), midline length (AE length) and area anterior pharyngeal endoderm (AE area) from the first pouch to the anterior most end of the pharyngeal endoderm (Fig. 5E). We normalized for ethanol-induced general growth deficits to anterior

pharyngeal endoderm shape, by measuring the length and width of the embryonic head and calculating head area (Fig. 5F). Calculating head area controls for ethanol-induced reductions in eye size and did not show any differences between groups (Fig. 5I). Our analyses showed a significant increase in AE area expressed as a ratio to head area in ethanol-treated double-homozygous *bmp4*$^{-/-}$;*smad5*$^{-/-}$ larva compared to all other groups (Fig. 5G, Table 3). AE area alone of ethanol-treated *bmp4*$^{-/-}$;*smad5*$^{-/-}$ larvae only exhibited a significant increase compared to ethanol-treated wild type, *bmp4*$^{+/+}$;*smad5*$^{+/+}$ larvae (Fig. 5H, Table 3). We also observed trends in linear measures with ethanol-treated *bmp4*$^{-/-}$;*smad5*$^{-/-}$ larvae showing increases in AE length and AE width while no differences were observed in head length and width (Supp. Fig. 1, Supp. Table 2). Collectively, our observations document that changes in anterior pharyngeal endoderm area in ethanol-treated Bmp mutants may underlie viscerocranial malformations.

Previous work has shown that the anterior pharyngeal endoderm is necessary to induce signaling factor expression in the oral ectoderm (Balczerski et al., 2012; Haworth et al., 2007, 2004). To test if expression of the critical oral ectoderm marker *fgf8a* is altered in ethanol-treated *bmp4*$^{-/-}$;*smad5*$^{-/-}$ larvae, we applied fluorescent *in situ* hybridization. In wild type embryos, *fgf8a* is expressed in a small domain ventro-posterior to the developing eye and retina (Fig. 6A). This expression domain of *fgf8a* was not altered in untreated *bmp4*$^{-/-}$;*smad5*$^{-/-}$ and ethanol-treated wild type, *bmp4*$^{+/+}$;*smad5*$^{+/+}$ larva (Fig. 6B-C). In contrast, *fgf8a* expression in ethanol-treated *bmp4*$^{-/-}$;*smad5*$^{-/-}$ larvae was expanded anteriorly to the level of developing the retina (Fig. 6D). Our data of ethanol-induced changes upon Bmp signaling perturbation to the *fgf8a* expression domain in the oral ectoderm is consistent with previous work showing that malformations of the anterior pharyngeal endoderm disrupting oral ectoderm expression domains and subsequent viscerocranial malformations (Balczerski et al., 2012). While limited to *fgf8* as critical marker, these observations indicate that synergistic Bmp-ethanol perturbations disrupt an anterior pharyngeal endoderm-oral ectoderm-signaling axis.

**Bmp-ethanol interactions are conserved in human**

Zebrafish has been used successfully to model human developmental disorders (Lieschke and Currie, 2007; Santoriello and Zon, 2012) and we have previously shown that our zebrafish screens can predict gene-ethanol interactions in humans (McCarthy et al., 2013). This suggests that our zebrafish model of

Bmp-ethanol interactions impacting facial shape may be predictive of gene-ethanol associations in humans. From a study of children recruited with and without prenatal alcohol exposure (PAE), we screened variants in human *BMP2*, *BMP4*, and *BMPR1B* to explore if mandible volume was associated with genotype in the presence or absence of ethanol. Only one SNP in the 5' region of *BMP2* (rs235710) was significant (p=0.029); no other SNPs in or near *BMP2* were correlated or demonstrated association (all p>0.74). Similarly, one SNP in the 5' region of *BMP4* (rs72680543, p=0.043) was significant but was in complete linkage disequilibrium (LD) (D'=1) with two SNPs that were non-significant (rs72680541, p=0.19; rs10873077, p=0.072). Given the lack of supporting evidence, we did not follow up on the findings in these two genes. The best p-value for SNPs in the BMP receptor gene *BMPR1B* was for rs34063820 (genotype by PAE interaction p=4.0x10-4, MAF=0.12; purple diamond in Fig. 7A). However, this result was not supported as there were no significant SNPs in strong LD with rs34063820. We therefore focused on a cluster of nine SNPs, which were in modest LD with rs34063820 (r2<0.60). These SNPs also demonstrated association with mandible volume that differed according to PAE. The best genotype by PAE interaction in these nine SNPs was for rs4397000 (purple diamond in Fig. 7B, p=0.016, all nine SNPs p<0.037).The rs4397000 SNP had a minor allele (A>C allele) frequency of 0.209 in the European Ancestry (EA) sample and 0.496 in the African Ancestry (AA) sample. Eight of the nine SNPs are eQTLs, expressing *BMPR1B* in several tissues. The minor allele A of rs4397000 increases *BMPR1B* gene expression in the adrenal gland but decreases expression in the brain, heart, and pancreas. The Wilcoxon test revealed that of those with an AA or AC genotype, there was no difference in mandible volume between the PAE (EA n=29, AA n=38) and no PAE (EA n=41, AA n=62) individuals, though mandible volume was trending toward significance in the AA samples (EA p=0.70, AA p=0.052; Fig. 8). However, in EA individuals with two copies of the C allele, those without PAE (EA n=52, AA n=15; Fig. 8) had larger mandible volume on average than those with PAE (EA n=64, p=0.040; AA n=19, p=0.53). Furthermore, EA individuals with PAE with an AA or AC genotype had larger mandible volume than those who were CC (EA p=0.0058, AA p=0.108; Fig. 8). All comparisons are shown in Fig. 8. This suggests that gene-ethanol interactions in the Bmp pathway potentially underlie abnormal jaw size in FASD. Taken together, our results demonstrate the predictive value of our mechanistic studies underlying FASD etiology in zebrafish.

## Discussion

Formation of the facial skeleton is driven by a complex, highly coordinated, three-dimensional process involving multiple tissues in the developing head (Francis-West et al., 2003; Murillo-Rincón and Kaucka, 2020). Proper regulation of the cell movements and tissue dynamics within a single tissue and between different tissues are critical for these events (Francis-West et al., 2003; Murillo-Rincón and Kaucka, 2020). These cell behaviors are regulated by numerous signaling pathways, which can be attenuated either genetically and/or environmentally, leading to a cascading effect that disrupts craniofacial development (Francis-West et al., 2003; Murillo-Rincón and Kaucka, 2020). Prenatal ethanol exposure, defined as FASD, results in a highly variable set phenotypes to the facial skeleton, including the jaw (Basart et al., 2018; Blanck-Lubarsch et al., 2020; Dörrie et al., 2014; Naidoo et al., 2005; Wozniak et al., 2019). Genetic risk factors lie at the heart of and are major drivers of FASD etiology, providing insight into the cellular and molecular processes potentially disrupted in FASD (Eberhart and Parnell, 2016; Lovely, 2020).

Here, we show that mutation in several components of the Bmp pathway sensitize embryos to ethanol induced malformations to the viscerocranium. We found that when exposed to ethanol from 10-18 hpf, mutations in *bmp2b*, *bmp4* and *bmpR1bb*, sensitize embryos to a range of ethanol-induced defects to Meckel's cartilages. These defects spanned reductions in size to outright loss of cartilage elements which broadly impacted overall impacted to shape of the viscerocranium with ethanol-treated Bmp mutants. Using a morphometric approach, we were able to observe broad changes to facial shape in ethanol-treated Bmp mutants. Ethanol-treated larva displaying a shorter and wider face relative to untreated controls and a flattening of the angles of several cartilage elements. Much of this variation was not identified in our initial screens supporting that this approach will identify subtle phenotypes impacting facial shape that would be missed if simply measuring cartilage size. Importantly, these broad ethanol-induced facial shape changes in zebrafish are consistent with analyses in human patients where alcohol exposed individuals showed facial shaped changes compared to age-matched controls (Suttie et al., 2013). Overall, this data documents that our morphometric analysis in zebrafish improve the rigor of identifying and quantifying ethanol-induced subtle facial shape changes, modeling the highly variable ethanol-induced facial shape changes in human studies.

Our results strongly suggest a synergistic interaction between Bmp and ethanol as neither condition alone generates the broad viscerocranial malformations observed in combination. Exacerbation of facial phenotypes in *bmp;smad5* double mutants demonstrates that dose-dependent reduction in Bmp signaling drives ethanol-induced phenotypes, suggesting that ethanol reduces signaling in the Bmp pathway. However, at what level of the Bmp pathway ethanol disrupts signaling is unknown. In the adult mouse liver, ethanol exposure decreases phosphorylation levels of Bmp type I receptors, BmpR1, and Smad1,5 while gene expression levels of the Bmp ligands, *Bmp2, Bmp4* and *Bmp6,* were increased (Gerjevic et al., 2012). This suggests that ethanol reduces Bmp receptor and Smad1/5/9 phosphorylation levels, but not gene expression of pathway components, leading to decreases in expression of Bmp target genes. Future work will determine at what level ethanol attenuates Bmp signaling.

**Impact of ethanol on pharyngeal endoderm morphogenesis**

Work in multiple model systems has shown that disruption to endoderm morphogenesis, in particular the anterior pharyngeal endoderm, leads to jaw defects (Balczerski et al., 2012; Chong Pyo Choe and Crump, 2015; Couly et al., 2002; Crump, 2004a; David et al., 2002; Haworth et al., 2004, 2007). This role for the anterior endoderm in jaw development may be indirect, by inducing signaling factor expression, such as *fgf8a*, in the oral ectoderm (Balczerski et al., 2012; Eberhart et al., 2006; Haworth et al., 2007, 2004; Hu, 2003). We have previously shown that Bmp signaling is required for pharyngeal endoderm morphogenesis from 10-18 hpf, the same as our ethanol-sensitive time window (Lovely et al., 2016). Consistent with this, we show that our Bmp-ethanol interactions alter anterior pharyngeal endoderm shape, increasing the area of the anterior pharyngeal endoderm relative to head size. Consistent with this increase in anterior pharyngeal endoderm size the *fgf8a* expression domain in the oral ectoderm was expanded. Strikingly, this increase in anterior pharyngeal endoderm size stands at odds with the decreases we observed in jaw shape and size. This suggests that the Bmp-ethanol interaction disrupts jaw formation through this endoderm-oral ectoderm-signaling axis. However, how this increase in anterior pharyngeal endoderm size results in a smaller jaw remains unclear and will require future work to determine.

Signaling centers in the pharyngeal endoderm directly pattern jaw formation and disruption to these signaling centers results in jaw hypoplasia (Couly et al., 2002; Vieux-Rochas et al., 2010). These signaling

centers are critical for survival of the neural crest with disruptions to endoderm morphogenesis leading to neural crest cell death (Edlund et al., 2014; Johnson et al., 2011; Kopinke et al., 2006). It is possible that ethanol-induced increases in the anterior endoderm size we observed alters signaling centers in both the anterior pharyngeal endoderm and the oral ectoderm. This would lead to increased cell death in the neural crest, resulting in decreased neural crest cell contribution to the forming jaw decreasing it size (Suzuki et al., 1999). While are data supports this hypothesis, more work needs to be done to analyze the impact of ethanol on endoderm-oral ectoderm-neural crest interactions driving jaw formation.

Pharyngeal endoderm formation requires highly coordinated cell movements and regulation of cell adhesion (Choe et al., 2013; Choe and Crump, 2014; C. P. Choe and Crump, 2015; Lovely et al., 2016). Driving these cell movements are actin dynamics, cell polarity and adhesion (Balaraju et al., 2021; Hu et al., 2018). Bmp signaling has been shown to regulate cell migration through actin dynamics and cell adhesion (Saxena et al., 2018; von der Hardt et al., 2007; Wen et al., 2007). This suggests that Bmp signaling may be regulating anterior endoderm morphogenesis by regulating the actin-based cell migration and adhesion and ethanol may be disrupting these events. Previous work has shown that ethanol can disrupt actin-based cell migration and points of cell adhesion (Dou et al., 2018; Iwata et al., 2011; Oyedele and Kramer, 2013; Rovasio and Battiato, 2002; Sarmah and Marrs, 2013). Ethanol-induced disruptions to these cell dynamics could lead to increased size of the anterior pharyngeal endoderm. Future work examining the dynamics of migrating cell will be needed to determine the impact of Bmp-ethanol interactions on anterior pharyngeal endoderm morphogenesis.

**Zebrafish model gene-ethanol interactions in human FASD**

We have previously shown that our zebrafish screens can predict gene-ethanol interactions in humans suggesting that our Bmp-ethanol interactions impacting facial shape may also be predictive of gene-ethanol associations in humans (McCarthy et al., 2013). Consistent with this, disruption of *Bmp2* (*BMP2*) in mice and human, in the absence of ethanol, results in a hypoplastic jaw (Chen et al., 2019; Sahoo et al., 2011). From a study of children recruited with and without prenatal alcohol exposure (PAE), we showed that several SNPs in *BMPR1B* are significantly associated with ethanol-associated jaw malformations. Jaw hypoplasia is commonly observed in FASD (Basart et al., 2018; Blanck-Lubarsch et al., 2020; Naidoo et

al., 2005) but studying FASD in humans is incredibly challenging due to the complex interplay between genetic background and ethanol timing and dosage. Our results show that zebrafish analyses can model gene-ethanol associations in humans and generate a deeper mechanistic understanding of gene-ethanol interactions on craniofacial development. While future human and zebrafish analyses will need to test for a causal relationship and the mechanistic underpinnings of ethanol-induced jaw deformations, this work strongly suggests that jaw malformations in FASD may in part be due to disruptions to epithelial dynamics and signaling events.

Combined, our results show that zebrafish can predict Bmp-ethanol associations in human and provide a valuable model system for determining the ethanol-sensitive tissue events that contribute to facial defects in FASD. However, despite our increased understanding of the clinical impact of prenatal ethanol exposure, much remains to be learned of the cellular mechanisms underlying FASD (Lovely, 2020). Our work here provides some of the first evidence of gene-ethanol interactions altering epithelial dynamics leading to facial malformations. This expands our current understanding of ethanol-sensitive tissue dynamics in FASD and provides a conceptual framework for future FASD studies. Ultimately, this work generates a mechanistic paradigm of ethanol-induced structural birth defects and connects ethanol exposure with concrete cellular events that could be sensitive beyond the jaw.

**Acknowledgements**

The authors like to thank Kevin Kump for animal care and husbandry. We thank Dr. Jim Amatruda for the providing the *bmpr1bb* zebrafish line. We also thank Dr. Duygu Özpolat and Dr. Ryan Hull for providing script for HCR probe design. We thank Dr. Christian Mosimann for manuscript editing. This work was funded by National Institutes of Health/National Institute on Alcohol Abuse (NIH/NIAAA) R00AA023560 to CBL, U01AA014809 to TF, U24AA030169 to LW, and U01AA014809 to MS. The genetic data utilized in the CIFASD cohort are available at https://cifasd.org/data-sharing/.

**Conflicts of Interest**

The authors declare that they have no competing interests.

## Author Contributions

CBL and JRK designed all zebrafish studies; JRK, RG, HV, GC, TS, LW, MA, MS and CBL conducted experiments and acquired data; JRK and CBL analyzed zebrafish data and wrote the manuscript; LW, TS, MA and MS designed all human studies, analyzed human data and assisted with writing the manuscript; all authors have read and approved the final manuscript.

## Ethic Approval

This study was approved by the Institutional Animal Care and Use Committee at the University of Louisville (protocol number IACUC 21875) and conducted in accordance with The Zebrafish Book, 5$^{th}$ Edition (Westerfield, 2007) and *the Guide for the Care and Use of Laboratory Animals* of the National Institutes of Health. All zebrafish were housed in IACUC-approved housing conditions. All human participants and/or their parents/legal guardians provided written informed consent and Institutional Review Board approval was obtained at each recruiting site.

## References


Arnold, J.S., 2006. Inactivation of Tbx1 in the pharyngeal endoderm results in 22q11DS malformations. Development 133, 977–987. https://doi.org/10.1242/dev.02264

Balaraju, A.K., Hu, B., Rodriguez, J.J., Murry, M., Lin, F., 2021. Glypican 4 regulates planar cell polarity of endoderm cells by controlling the localization of Cadherin 2. Development 148, dev199421. https://doi.org/10.1242/dev.199421

Balczerski, B., Matsutani, M., Castillo, P., Osborne, N., Stainier, D.Y.R., Crump, J.G., 2012. Analysis of Sphingosine-1-phosphate signaling mutants reveals endodermal requirements for the growth but not dorsoventral patterning of jaw skeletal precursors. Developmental Biology 362, 230–241. https://doi.org/10.1016/j.ydbio.2011.12.010

Basart, H., Suttie, M., Ibrahim, A., Ferretti, P., Van Der Horst, C.M.A.M., Hennekam, R.C., Hammond, P., 2018. Objectifying Micrognathia Using Three-Dimensional Photogrammetric Analysis: Journal of Craniofacial Surgery 29, 2106–2109. https://doi.org/10.1097/SCS.0000000000005056

Bilotta, J., Barnett, J.A., Hancock, L., Saszik, S., 2004. Ethanol exposure alters zebrafish development: A novel model of fetal alcohol syndrome. Neurotoxicology and Teratology 26, 737–743. https://doi.org/10.1016/j.ntt.2004.06.011

Blanck-Lubarsch, M., Dirksen, D., Feldmann, R., Sauerland, C., Kirschneck, C., Hohoff, A., 2020. Asymmetry-index and orthodontic facial analysis of children with foetal alcohol syndrome using 3D-facial scans. Pediatr Res 88, 243–249. https://doi.org/10.1038/s41390-019-0559-5

Boyles, A.L., DeRoo, L.A., Lie, R.T., Taylor, J.A., Jugessur, A., Murray, J.C., Wilcox, A.J., 2010. Maternal Alcohol Consumption, Alcohol Metabolism Genes, and the Risk of Oral Clefts: A Population-based Case-Control Study in Norway, 1996-2001. American Journal of Epidemiology 172, 924–931. https://doi.org/10.1093/aje/kwq226

Canfield, D.V., Forster, E.M., Cheong, Z.-I., Cowan, J.M., 2019. Breath/Blood Alcohol Concentration as an Indicator of Alcohol Use Problems. Aerospace Medicine and Human Performance 90, 488–491. https://doi.org/10.3357/AMHP.5256.2019

Chen, Yixuan, Wang, Z., Chen, YiPing, Zhang, Y., 2019. Conditional deletion of Bmp2 in cranial neural crest cells recapitulates Pierre Robin sequence in mice. Cell Tissue Res 376, 199–210. https://doi.org/10.1007/s00441-018-2944-5

Choe, C.P., Collazo, A., Trinh, L.A., Pan, L., Moens, C.B., Crump, J.G., 2013. Wnt-Dependent Epithelial Transitions Drive Pharyngeal Pouch Formation. Developmental Cell 24, 296–309. https://doi.org/10.1016/j.devcel.2012.12.003

Choe, Chong Pyo, Crump, J.G., 2015. Dynamic epithelia of the developing vertebrate face. Current Opinion in Genetics & Development 32, 66–72. https://doi.org/10.1016/j.gde.2015.02.003

Choe, C. P., Crump, J.G., 2015. Eph-Pak2a signaling regulates branching of the pharyngeal endoderm by inhibiting late-stage epithelial dynamics. Development 142, 1089–1094. https://doi.org/10.1242/dev.115774

Choe, C.P., Crump, J.G., 2014. Tbx1 controls the morphogenesis of pharyngeal pouch epithelia through mesodermal Wnt11r and Fgf8a. Development 141, 3583–3593. https://doi.org/10.1242/dev.111740

Chung, W.-S., Stainier, D.Y.R., 2008a. Intra-Endodermal Interactions Are Required for Pancreatic β Cell Induction. Developmental Cell 14, 582–593. https://doi.org/10.1016/j.devcel.2008.02.012

Chung, W.-S., Stainier, D.Y.R., 2008b. Intra-Endodermal Interactions Are Required for Pancreatic β Cell Induction. Developmental Cell 14, 582–593. https://doi.org/10.1016/j.devcel.2008.02.012

Clouthier, D.E., Schilling, T.F., 2004. Understanding endothelin-1 function during craniofacial development in the mouse and zebrafish. Birth Defect Res C 72, 190–199. https://doi.org/10.1002/bdrc.20007

Cordero, D.R., Brugmann, S., Chu, Y., Bajpai, R., Jame, M., Helms, J.A., 2011. Cranial neural crest cells on the move: Their roles in craniofacial development. Am. J. Med. Genet. 155, 270–279. https://doi.org/10.1002/ajmg.a.33702

Couly, G., Creuzet, S., Bennaceur, S., Vincent, C., Le Douarin, N.M., 2002. Interactions between Hox-negative cephalic neural crest cells and the foregut endoderm in patterning the facial skeleton in the vertebrate head. Development 129, 1061–1073.

Crump, J.G., 2004a. An essential role for Fgfs in endodermal pouch formation influences later craniofacial skeletal patterning. Development 131, 5703–5716. https://doi.org/10.1242/dev.01444

Crump, J.G., 2004b. An essential role for Fgfs in endodermal pouch formation influences later craniofacial skeletal patterning. Development 131, 5703–5716. https://doi.org/10.1242/dev.01444

Das, S., Forer, L., Schönherr, S., Sidore, C., Locke, A.E., Kwong, A., Vrieze, S.I., Chew, E.Y., Levy, S., McGue, M., Schlessinger, D., Stambolian, D., Loh, P.-R., Iacono, W.G., Swaroop, A., Scott, L.J., Cucca, F., Kronenberg, F., Boehnke, M., Abecasis, G.R., Fuchsberger, C., 2016. Next-generation genotype imputation service and methods. Nat Genet 48, 1284–1287. https://doi.org/10.1038/ng.3656

David, N.B., Saint-Etienne, L., Tsang, M., Schilling, T.F., Rosa, F.M., 2002. Requirement for endoderm and FGF3 in ventral head skeleton formation. Development 129, 4457–4468. https://doi.org/10.1242/dev.129.19.4457

Depew, M.J., Lufkin, T., Rubenstein, J.L.R., 2002. Specification of Jaw Subdivisions by Dlx Genes. Science 298, 381–385. https://doi.org/10.1126/science.1075703

Dörrie, N., Föcker, M., Freunscht, I., Hebebrand, J., 2014. Fetal alcohol spectrum disorders. Eur Child Adolesc Psychiatry 23, 863–875. https://doi.org/10.1007/s00787-014-0571-6

Dou, X., Menkari, C., Mitsuyama, R., Foroud, T., Wetherill, L., Hammond, P., Suttie, M., Chen, X., Chen, S., Charness, M.E., Collaborative Initiative On Fetal A, 2018. L1 coupling to ankyrin and the spectrin- actin cytoskeleton modulates ethanol inhibition of L1 adhesion and ethanol teratogenesis. FASEB j. 32, 1364–1374. https://doi.org/10.1096/fj.201700970

Eberhart, J.K., Parnell, S.E., 2016. The Genetics of Fetal Alcohol Spectrum Disorders. Alcohol Clin Exp Res 40, 1154–1165. https://doi.org/10.1111/acer.13066

Eberhart, J.K., Swartz, M.E., Crump, J.G., Kimmel, C.B., 2006. Early Hedgehog signaling from neural to oral epithelium organizes anterior craniofacial development. Development 133, 1069–1077. https://doi.org/10.1242/dev.02281

Edlund, R.K., Ohyama, T., Kantarci, H., Riley, B.B., Groves, A.K., 2014. Foxi transcription factors promote pharyngeal arch development by regulating formation of FGF signaling centers. Developmental Biology 390, 1–13. https://doi.org/10.1016/j.ydbio.2014.03.004

Ethen, M.K., Ramadhani, T.A., Scheuerle, A.E., Canfield, M.A., Wyszynski, D.F., Druschel, C.M., Romitti, P.A., National Birth Defects Prevention Study, 2009. Alcohol Consumption by Women Before and During Pregnancy. Matern Child Health J 13, 274–285. https://doi.org/10.1007/s10995-008-0328-2

Everson, J.L., Batchu, R., Eberhart, J.K., 2020. Multifactorial Genetic and Environmental Hedgehog Pathway Disruption Sensitizes Embryos to Alcohol- Induced Craniofacial Defects. Alcohol Clin. Exp. Res. 44, 1988–1996. https://doi.org/10.1111/acer.14427

Everson, J.L., Tseng, Y., Eberhart, J.K., 2022. High-throughput detection of craniofacial defects in fluorescent zebrafish. Birth Defects Research bdr2.2127. https://doi.org/10.1002/bdr2.2127

Fairley, S., Lowy-Gallego, E., Perry, E., Flicek, P., 2020. The International Genome Sample Resource (IGSR) collection of open human genomic variation resources. Nucleic Acids Research 48, D941–D947. https://doi.org/10.1093/nar/gkz836

Fernandes, Y., Lovely, C.B., 2021. Zebrafish models of fetal alcohol spectrum disorders. genesis 59. https://doi.org/10.1002/dvg.23460

Flentke, G.R., Klingler, R.H., Tanguay, R.L., Carvan, M.J., Smith, S.M., 2014. An Evolutionarily Conserved Mechanism of Calcium-Dependent Neurotoxicity in a Zebrafish Model of Fetal Alcohol Spectrum Disorders. Alcohol Clin Exp Res 38, 1255–1265. https://doi.org/10.1111/acer.12360

Francis-West, P.H., Robson, L., Evans, D.J.R., 2003. Craniofacial Development The Tissue and Molecular Interactions That Control Development of the Head, Advances in Anatomy, Embryology and Cell Biology. Springer Berlin Heidelberg, Berlin, Heidelberg. https://doi.org/10.1007/978-3-642-55570-1

Gerjevic, L.N., Liu, N., Lu, S., Harrison-Findik, D.D., 2012. Alcohol Activates TGF-Beta but Inhibits BMP Receptor-Mediated Smad Signaling and Smad4 Binding to Hepcidin Promoter in the Liver. International Journal of Hepatology 2012, 1–11. https://doi.org/10.1155/2012/459278

Haworth, K.E., Healy, C., Morgan, P., Sharpe, P.T., 2004. Regionalisation of early head ectoderm is regulated by endoderm and prepatterns the orofacial epithelium. Development 131, 4797–4806. https://doi.org/10.1242/dev.01337

Haworth, K.E., Wilson, J.M., Grevellec, A., Cobourne, M.T., Healy, C., Helms, J.A., Sharpe, P.T., Tucker, A.S., 2007. Sonic hedgehog in the pharyngeal endoderm controls arch pattern via regulation of Fgf8 in head ectoderm. Developmental Biology 303, 244–258. https://doi.org/10.1016/j.ydbio.2006.11.009

Hong, M., Krauss, R.S., 2012. Cdon Mutation and Fetal Ethanol Exposure Synergize to Produce Midline Signaling Defects and Holoprosencephaly Spectrum Disorders in Mice. PLoS Genet 8, e1002999. https://doi.org/10.1371/journal.pgen.1002999

Hu, B., Gao, Y., Davies, L., Woo, S., Topczewski, J., Jessen, J.R., Lin, F., 2018. Glypican 4 and Mmp14 interact in regulating the migration of anterior endodermal cells by limiting extracellular matrix deposition. Development 145, dev163303. https://doi.org/10.1242/dev.163303

Hu, D., 2003. A zone of frontonasal ectoderm regulates patterning and growth in the face. Development 130, 1749–1758. https://doi.org/10.1242/dev.00397

Ibarra-García-Padilla, R., Howard, A.G.A., Singleton, E.W., Uribe, R.A., 2021. A protocol for whole-mount immuno-coupled hybridization chain reaction (WICHCR) in zebrafish embryos and larvae. STAR Protocols 2, 100709. https://doi.org/10.1016/j.xpro.2021.100709

Iwata, T., Nozu, F., Imawari, M., 2011. Ethanol impairs the assembly and disassembly of actin cytoskeleton and cell adhesion via the RhoA signaling pathway, catenin p120 and E-cadherin in CCK-stimulated pancreatic acini. Biochemical and Biophysical Research Communications 405, 558–563. https://doi.org/10.1016/j.bbrc.2011.01.067

Johnson, C.W., Hernandez-Lagunas, L., Feng, W., Melvin, V.S., Williams, T., Artinger, K.B., 2011. Vgll2a is required for neural crest cell survival during zebrafish craniofacial development. Developmental Biology 357, 269–281. https://doi.org/10.1016/j.ydbio.2011.06.034

Jones, A.W., 2008. Ultra-rapid rate of ethanol elimination from blood in drunken drivers with extremely high blood-alcohol concentrations. Int J Legal Med 122, 129–134. https://doi.org/10.1007/s00414-007-0181-7

Klingenberg, C.P., 2011. MorphoJ: an integrated software package for geometric morphometrics: COMPUTER PROGRAM NOTE. Molecular Ecology Resources 11, 353–357. https://doi.org/10.1111/j.1755-0998.2010.02924.x

Knight, R.D., Schilling, T.F., 2006. Cranial Neural Crest and Development of the Head Skeleton, in: Saint-Jeannet, J.-P. (Ed.), Neural Crest Induction and Differentiation, Advances in Experimental Medicine and Biology. Springer US, Boston, MA, pp. 120–133. https://doi.org/10.1007/978-0-387-46954-6_7

Kondo, M., 2007. Bone morphogenetic proteins in the early development of zebrafish: BMPs in the early development of zebrafish. FEBS Journal 274, 2960–2967. https://doi.org/10.1111/j.1742-4658.2007.05838.x

Kopinke, D., Sasine, J., Swift, J., Stephens, W.Z., Piotrowski, T., 2006. Retinoic acid is required for endodermal pouch morphogenesis and not for pharyngeal endoderm specification. Dev. Dyn. 235, 2695–2709. https://doi.org/10.1002/dvdy.20905

Kuehn, E., Clausen, D.S., Null, R.W., Metzger, B.M., Willis, A.D., Özpolat, B.D., 2022. Segment number threshold determines juvenile onset of germline cluster expansion in *Platynereis dumerilii*. J Exp Zool Pt B 338, 225–240. https://doi.org/10.1002/jez.b.23100

Langevin, F., Crossan, G.P., Rosado, I.V., Arends, M.J., Patel, K.J., 2011. Fancd2 counteracts the toxic effects of naturally produced aldehydes in mice. Nature 475, 53–58. https://doi.org/10.1038/nature10192

Li, L., Lin, M., Wang, Y., Cserjesi, P., Chen, Z., Chen, Y., 2011. BmprIa is required in mesenchymal tissue and has limited redundant function with BmprIb in tooth and palate development. Developmental Biology 349, 451–461. https://doi.org/10.1016/j.ydbio.2010.10.023

Li, L., Ning, G., Yang, S., Yan, Y., Cao, Y., Wang, Q., 2019. BMP signaling is required for nkx2.3-positive pharyngeal pouch progenitor specification in zebrafish. PLoS Genet 15, e1007996. https://doi.org/10.1371/journal.pgen.1007996

Lieschke, G.J., Currie, P.D., 2007. Animal models of human disease: zebrafish swim into view. Nat Rev Genet 8, 353–367. https://doi.org/10.1038/nrg2091

Little, S.C., Mullins, M.C., 2009. Bone morphogenetic protein heterodimers assemble heteromeric type I receptor complexes to pattern the dorsoventral axis. Nat Cell Biol 11, 637–643. https://doi.org/10.1038/ncb1870

Liu, W., Selever, J., Murali, D., Sun, X., Brugger, S.M., Ma, L., Schwartz, R.J., Maxson, R., Furuta, Y., Martin, J.F., 2005. Threshold-specific requirements for Bmp4 in mandibular development. Developmental Biology 283, 282–293. https://doi.org/10.1016/j.ydbio.2005.04.019

Lovely, C.B., 2020. Animal models of gene–alcohol interactions. Birth Defects Research 112, 367–379. https://doi.org/10.1002/bdr2.1623

Lovely, C.B., Nobles, R.D., Eberhart, J.K., 2014. Developmental age strengthens barriers to ethanol accumulation in zebrafish. Alcohol 48, 595–602. https://doi.org/10.1016/j.alcohol.2014.06.003

Lovely, C.B., Swartz, M.E., McCarthy, N., Norrie, J.L., Eberhart, J.K., 2016. Bmp signaling mediates endoderm pouch morphogenesis by regulating Fgf signaling in zebrafish. Development 143, 2000–2011. https://doi.org/10.1242/dev.129379

Maier, S.E., 2001. Drinking Patterns and Alcohol-Related Birth Defects 25, 7.

Mattson, S.N., Foroud, T., Sowell, E.R., Jones, K.L., Coles, C.D., Fagerlund, Å., Autti-Rämö, I., May, P.A., Adnams, C.M., Konovalova, V., Wetherill, L., Arenson, A.D., Barnett, W.K., Riley, E.P., 2010a. Collaborative initiative on fetal alcohol spectrum disorders: methodology of clinical projects. Alcohol 44, 635–641. https://doi.org/10.1016/j.alcohol.2009.08.005

Mattson, S.N., Roesch, S.C., Fagerlund, Å., Autti-Rämö, I., Jones, K.L., May, P.A., Adnams, C.M., Konovalova, V., Riley, E.P., the CIFASD, 2010b. Toward a Neurobehavioral Profile of Fetal Alcohol Spectrum Disorders: NEUROBEHAVIORAL PROFILE OF FETAL ALCOHOL SPECTRUM DISORDERS. Alcoholism: Clinical and Experimental Research 34, 1640–1650. https://doi.org/10.1111/j.1530-0277.2010.01250.x

McCarthy, N., Wetherill, L., Lovely, C.B., Swartz, M.E., Foroud, T.M., Eberhart, J.K., 2013. Pdgfra protects against ethanol-induced craniofacial defects in a zebrafish model of FASD. Development 140, 3254–3265. https://doi.org/10.1242/dev.094938

Mork, L., Crump, G., 2015. Zebrafish Craniofacial Development, in: Current Topics in Developmental Biology. Elsevier, pp. 235–269. https://doi.org/10.1016/bs.ctdb.2015.07.001

Mu, H., Liu, X., Geng, S., Su, D., Chang, H., Li, L., Jin, H., Wang, X., Li, Y., Zhang, B., Xie, X., 2021. Epithelial Bone Morphogenic Protein 2 and 4 Are Indispensable for Tooth Development. Front. Physiol. 12, 660644. https://doi.org/10.3389/fphys.2021.660644

Muggli, E., Matthews, H., Penington, A., Claes, P., O'Leary, C., Forster, D., Donath, S., Anderson, P.J., Lewis, S., Nagle, C., Craig, J.M., White, S.M., Elliott, E.J., Halliday, J., 2017. Association Between Prenatal Alcohol Exposure and Craniofacial Shape of Children at 12 Months of Age. JAMA Pediatr 171, 771. https://doi.org/10.1001/jamapediatrics.2017.0778

Mullins, M.C., Hammerschmidt, M., Kane, D.A., Odenthal, J., Brand, M., 1996. Genes establishing dorsoventral pattern formation in the zebrafish embryo: the ventral specifying genes. Development 123, 13.

Murillo-Rincón, A.P., Kaucka, M., 2020. Insights Into the Complexity of Craniofacial Development From a Cellular Perspective. Front. Cell Dev. Biol. 8, 620735. https://doi.org/10.3389/fcell.2020.620735

Naidoo, S., Harris, A., Swanevelder, S., Lombard, C., 2005. Foetal alcohol syndrome: a cephalometric analysis of patients and controls. The European Journal of Orthodontics 28, 254–261. https://doi.org/10.1093/ejo/cji110

Neumann, J.C., Chandler, G.L., Damoulis, V.A., Fustino, N.J., Lillard, K., Looijenga, L., Margraf, L., Rakheja, D., Amatruda, J.F., 2011. Mutation in the type IB bone morphogenetic protein receptor *alk6b* impairs germ-cell differentiation and causes germ-cell tumors in zebrafish. Proc Natl Acad Sci USA 108, 13153–13158. https://doi.org/10.1073/pnas.1102311108

Nguyen, V.H., Schmid, B., Trout, J., Connors, S.A., Ekker, M., Mullins, M.C., 1998. Ventral and Lateral Regions of the Zebrafish Gastrula, Including the Neural Crest Progenitors, Are Established by abmp2b/swirlPathway of Genes. Developmental Biology 199, 93–110. https://doi.org/10.1006/dbio.1998.8927

Oyedele, O.O., Kramer, B., 2013. Nuanced but significant: How ethanol perturbs avian cranial neural crest cell actin cytoskeleton, migration and proliferation. Alcohol 47, 417–426. https://doi.org/10.1016/j.alcohol.2013.04.001

Reimers, M.J., Flockton, A.R., Tanguay, R.L., 2004. Ethanol- and acetaldehyde-mediated developmental toxicity in zebrafish. Neurotoxicology and Teratology 26, 769–781. https://doi.org/10.1016/j.ntt.2004.06.012

Rovasio, R.A., Battiato, N.L., 2002. Ethanol Induces Morphological and Dynamic Changes on In Vivo and In Vitro Neural Crest Cells. Alcoholism Clin Exp Res 26, 1286–1298. https://doi.org/10.1111/j.1530-0277.2002.tb02669.x

Sahoo, T., Theisen, A., Sanchez-Lara, P.A., Marble, M., Schweitzer, D.N., Torchia, B.S., Lamb, A.N., Bejjani, B.A., Shaffer, L.G., Lacassie, Y., 2011. Microdeletion 20p12.3 involving BMP2 contributes to syndromic forms of cleft palate. Am. J. Med. Genet. 155, 1646–1653. https://doi.org/10.1002/ajmg.a.34063

Santoriello, C., Zon, L.I., 2012. Hooked! Modeling human disease in zebrafish. J. Clin. Invest. 122, 2337–2343. https://doi.org/10.1172/JCI60434

Sarmah, S., Marrs, J.A., 2013. Complex cardiac defects after ethanol exposure during discrete cardiogenic events in zebrafish: Prevention with folic acid: FASD Cardiac Defects: Folic Acid Rescue. Dev. Dyn. 242, 1184–1201. https://doi.org/10.1002/dvdy.24015

Saxena, M., Agnihotri, N., Sen, J., 2018. Perturbation of canonical and non-canonical BMP signaling affects migration, polarity and dendritogenesis of mouse cortical neurons. Development 145, dev147157. https://doi.org/10.1242/dev.147157

Schille, C., Heller, J., Schambony, A., 2016. Differential requirement of bone morphogenetic protein receptors Ia (ALK3) and Ib (ALK6) in early embryonic patterning and neural crest development. BMC Dev Biol 16, 1. https://doi.org/10.1186/s12861-016-0101-5

Schindelin, J., Arganda-Carreras, I., Frise, E., Kaynig, V., Longair, M., Pietzsch, T., Preibisch, S., Rueden, C., Saalfeld, S., Schmid, B., Tinevez, J.-Y., White, D.J., Hartenstein, V., Eliceiri, K., Tomancak, P., Cardona, A., 2012. Fiji: an open-source platform for biological-image analysis. Nat Methods 9, 676–682. https://doi.org/10.1038/nmeth.2019

Schwantes-An, T., Darlay, R., Mathurin, P., Masson, S., Liangpunsakul, S., Mueller, S., Aithal, G.P., Eyer, F., Gleeson, D., Thompson, A., Muellhaupt, B., Stickel, F., Soyka, M., Goldman, D., Liang, T., Lumeng, L., Pirmohamed, M., Nalpas, B., Jacquet, J., Moirand, R., Nahon, P., Naveau, S., Perney, P., Botwin, G., Haber, P.S., Seitz, H.K., Day, C.P., Foroud, T.M., Daly, A.K., Cordell, H.J., Whitfield, J.B., Morgan, T.R., Seth, D., for the GenomALC Consortium, 2021. Genome-wide Association Study and Meta-analysis on Alcohol-Associated Liver Cirrhosis Identifies Genetic Risk Factors. Hepatology 73, 1920–1931. https://doi.org/10.1002/hep.31535

Stickney, H.L., Imai, Y., Draper, B., Moens, C., Talbot, W.S., 2007. Zebrafish bmp4 functions during late gastrulation to specify ventroposterior cell fates. Developmental Biology 14.

Suttie, M., Foroud, T., Wetherill, L., Jacobson, J.L., Molteno, C.D., Meintjes, E.M., Hoyme, H.E., Khaole, N., Riley, E.P., Jacobson, S.W., Hammond, P., 2013. Facial Dysmorphism Across the Fetal Alcohol Spectrum 131, 12.

Suzuki, T., Oohara, I., Kurokawa, T., 1999. Retinoic acid given at late embryonic stage depresses sonic hedgehog and Hoxd-4 expression in the pharyngeal area and induces skeletal malformation in

flounder (Paralichthys olivaceus) embryos. Dev Growth Differ 41, 143–152. https://doi.org/10.1046/j.1440-169x.1999.00420.x

Swartz, M.E., Lovely, C.B., McCarthy, N., Kuka, T., Eberhart, J.K., 2020. Novel Ethanol-Sensitive Mutants Identified in an F3 Forward Genetic Screen. Alcohol Clin Exp Res 44, 56–65. https://doi.org/10.1111/acer.14240

Swartz, M.E., Sheehan-Rooney, K., Dixon, M.J., Eberhart, J.K., 2011. Examination of a palatogenic gene program in zebrafish. Dev. Dyn. 240, 2204–2220. https://doi.org/10.1002/dvdy.22713

Swartz, M.E., Wells, M.B., Griffin, M., McCarthy, N., Lovely, C.B., McGurk, P., Rozacky, J., Eberhart, J.K., 2014. A Screen of Zebrafish Mutants Identifies Ethanol-Sensitive Genetic Loci. Alcohol Clin Exp Res 38, 694–703. https://doi.org/10.1111/acer.12286

Tajer, B., Dutko, J.A., Little, S.C., Mullins, M.C., 2021. BMP heterodimers signal via distinct type I receptor class functions. Proc Natl Acad Sci USA 118, e2017952118. https://doi.org/10.1073/pnas.2017952118

Trainor, P.A., Melton, K.R., Manzanares, M., 2003. Origins and plasticity of neural crest cells and their roles in jaw and craniofacial evolution. Int J Dev Biol 47, 13.

Vieux-Rochas, M., Mantero, S., Heude, E., Barbieri, O., Astigiano, S., Couly, G., Kurihara, H., Levi, G., Merlo, G.R., 2010. Spatio-temporal dynamics of gene expression of the Edn1-Dlx5/6 pathway during development of the lower jaw. Genesis 48, 262–373. https://doi.org/10.1002/dvg.20625

von der Hardt, S., Bakkers, J., Inbal, A., Carvalho, L., Solnica-Krezel, L., Heisenberg, C.-P., Hammerschmidt, M., 2007. The Bmp Gradient of the Zebrafish Gastrula Guides Migrating Lateral Cells by Regulating Cell-Cell Adhesion. Current Biology 17, 475–487. https://doi.org/10.1016/j.cub.2007.02.013

Walker, M., Kimmel, C., 2007. A two-color acid-free cartilage and bone stain for zebrafish larvae. Biotechnic & Histochemistry 82, 23–28. https://doi.org/10.1080/10520290701333558

Wen, Z., Han, L., Bamburg, J.R., Shim, S., Ming, G., Zheng, J.Q., 2007. BMP gradients steer nerve growth cones by a balancing act of LIM kinase and Slingshot phosphatase on ADF/cofilin. Journal of Cell Biology 178, 107–119. https://doi.org/10.1083/jcb.200703055

Westerfield, M., 2007. The zebrafish book. A guide for the laboratory use of zebrafish (Danio rerio), 5th ed.

Whaley, C.C., Young, M.M., Gaynor, B.G., 2019. Very High Blood Alcohol Concentration and Fatal Hemorrhage in Acute Subdural Hematoma. World Neurosurgery 130, 454–458. https://doi.org/10.1016/j.wneu.2019.06.124

Wise, S.B., Stock, D.W., 2010. bmp2b and bmp4 are dispensable for zebrafish tooth development. Dev. Dyn. 239, 2534–2546. https://doi.org/10.1002/dvdy.22411

Wozniak, J.R., Riley, E.P., Charness, M.E., 2019. Clinical presentation, diagnosis, and management of fetal alcohol spectrum disorder. The Lancet Neurology 18, 760–770. https://doi.org/10.1016/S1474-4422(19)30150-4

Zhang, C., Frazier, J.M., Chen, H., Liu, Y., Lee, J.-A., Cole, G.J., 2014. Molecular and morphological changes in zebrafish following transient ethanol exposure during defined developmental stages. Neurotoxicology and Teratology 44, 70–80. https://doi.org/10.1016/j.ntt.2014.06.001

Zhang, C., Ojiaku, P., Cole, G.J., 2013. Forebrain and hindbrain development in zebrafish is sensitive to ethanol exposure involving agrin, Fgf, and sonic hedgehog function. Birth Defects Research Part A: Clinical and Molecular Teratology 97, 8–27. https://doi.org/10.1002/bdra.23099

Zheng, X., Levine, D., Shen, J., Gogarten, S.M., Laurie, C., Weir, B.S., 2012. A high-performance computing toolset for relatedness and principal component analysis of SNP data. Bioinformatics 28, 3326–3328. https://doi.org/10.1093/bioinformatics/bts606

## Figure Legends

**Figure 1. Multiple members of the Bmp pathway display ethanol sensitive facial phenotypes.** (A-H) Whole-mount images of viscerocranium at 5 dpf larva. Cartilage is blue and bone is red (Ventral views, anterior to the left, scale bar: 100 µm, MC = Meckel's, Pq = palatoquadrate, Ch = ceratohyal and HM = hyomandibular cartilages). (I) Area measures of the Meckel's cartilage. (A-D) *bmp2b*$^{+/-}$ or *bmp4*$^{-/-}$ or *bmpr1bb*$^{-/-}$ larva develop comparable to Wild type larva. (E-H) Exposure of 1% ethanol exposure from 10-18 hpf results in a range of defects to the viscerocranium, from loss of MC (asterisks) to reductions in size and changes in shape in the MC (arrows) as well as a flattening of the Ch (arrowheads) in the Bmp mutant alleles but not in Wild type siblings. (I) The size Meckel's cartilage element was reduced in ethanol-treated *bmp2b*$^{+/-}$ larva compared to ethanol-treated *bmp2b*$^{+/+}$ and untreated *bmp2b*$^{+/-}$ larva (F=36.85, p=.0001, one-way ANOVA, n=58 cartilage elements per group).

**Figure 2. Ethanol exposure alters viscerocranial shape in *bmp4*$^{-/-}$ larva.** Landmarks were placed on several joints between the cartilage elements of the viscerocranium. Genotypes are color-coded; black = untreated *bmp4*$^{+/+}$ larva (n = 61), green = untreated *bmp4*$^{-/-}$ larva (n = 54), orange = ethanol-treated *bmp4*$^{+/+}$ larva (n = 58), magenta = ethanol-treated *bmp4*$^{-/-}$ larva (n = 66), dashed circles represent confidence ellipses in which 95% of all individual data points for each group lie, solid circles represent 95% confidence ellipses for means. Wireframe graphs represent variation described by each axis with black representing no variation and magenta representing variation relative to the black wireframe. For example, PC1 captures a shortening and widening in viscerocranial shape, while PC2 represents variation in midfacial width. Procrustes ANOVA showed significant change in the viscerocranial shape (F = 10.37, DF = 36, p = .0001).

**Figure 3. Ethanol exposure alters linear measures of viscerocranial shape in *bmp4*$^{-/-}$ larva.** (A, E) Whole-mount images of viscerocranium at 5 dpf larva showing linear measures and cartilage angles (cartilage is blue and bone is red, ventral views, anterior to the left). (B) Length measures between the midline joints of the Meckel's cartilages and ceratohyal cartilages and width measures between the joints of the (C) Meckel's and palatoquadrate cartilages and (D) ceratohyal and palatoquadrate cartilages. Measures of angles joint of the (F) Meckel's and (G) ceratohyal cartilages. Linear measures show

significant decrease in facial width and length and an increase in angle between cartilage elements, representing flattening of the facial skeleton (Orange = untreated *bmp4*$^{+/+}$ larva: n = 61, magenta = untreated *bmp4*$^{-/-}$ larva: n = 54), blue = ethanol-treated *bmp4*$^{+/+}$ larva: n = 58, rose = ethanol-treated *bmp4*$^{-/-}$ larva: n = 66, individual graph statistics in Table 2).

**Figure 4. Ethanol exposure alters area of the anterior pharyngeal endoderm in *bmp4*$^{-/-}$*;smad5*$^{-/-}$ larva.** (A-D) Whole-mount images of viscerocranium at 5 dpf larva. Cartilage is blue and bone is red (Ventral views, anterior to the left, scale bar: 100 µm). (A) No impact on facial formation was observed in untreated *bmp4*$^{-/-}$*;smad5*$^{+/-}$ larva. (B) Stereotypical *smad5* mutant phenotypes were observed in *bmp4*$^{-/-}$*;smad5*$^{-/-}$ larva. (C) Ethanol does not impact viscerocranial morphology in *bmp4*$^{-/-}$*;smad5*$^{+/-}$ larva. (D) However, *bmp4*$^{-/-}$*;smad5*$^{-/-}$ larva are fully penetrant, ethanol sensitive, resulting several viscerocranial malformations recapitulating the severe phenotypes in dorsomorphin-treated embryos (Lovely et al., 2016).

**Figure 5. Ethanol exposure alters area of the anterior pharyngeal endoderm in *bmp4*$^{-/-}$*;smad5*$^{-/-}$ larva.** (A-D) Whole-mount images of pharyngeal endoderm in 36 hpf embryos; (A'-D') zoomed in view of the anterior pharyngeal endoderm (Wild type control, n = 18, A, A'; *bmp4; smad5* mutant control, n = 20, B, B'; Wild type ethanol-treated, n = 12, C, C'; *bmp4; smad5* mutant ethanol-treated, n = 14, D, D'; dorsal views, anterior to the left; Size bars: 50 µm). (E) Area and length of the anterior pharyngeal endoderm was measured from the first pouch to the anterior-most tip while width of the anterior pharyngeal endoderm was measured at the level of the first pouch. (F) Area of the head was calculated from length (first pouch to most anterior tip of the head) and width (measured at the level of the first pouch) of the head. (G) Ratio of anterior pharyngeal endoderm to head area shows that ethanol-treated *bmp4; smad5* mutants show increased area of the anterior endoderm compared to all other groups. This increased size is not due to changes in head size (H) but due to increased size in the anterior pharyngeal endoderm directly (I, individual graph statistics in Table 3).

**Figure 6. Ethanol exposure changes shape of oral ectoderm expression domain in *bmp4*$^{-/-}$*;smad5*$^{-/-}$ larva.** (A-D) Whole-mount, confocal images of *bmp4;smad5;sox17:EGFP* embryos fluorescently labeling

*fgf8a* gene expression at 36 hpf (lateral views, anterior to the left, scale bar: 50 μm). (A-C) Arrows show normal expression of *fgf8a* in the oral ectoderm of untreated *bmp4*$^{+/+}$*;smad5*$^{+/+}$ and *bmp4*$^{-/-}$*;smad5*$^{-/-}$ embryos as well as ethanol-treated *bmp4*$^{+/+}$*;smad5*$^{+/+}$ embryos. (D) Arrowhead shows that domain of *fgf8a* expression in ethanol-treated *bmp4*$^{-/-}$*;smad5*$^{-/-}$ embryos is expanded anteriorly (n = 7 embryos per group).

**Figure 7. Association of jaw deformations with SNPs located between BMPR1B in a combined European and African American discovery sample.** (A-B) Y-axis denotes the -log10 (p-value) for the genotype x PAE effect. X-axis is the physical position on the chromosome (Mb). The extent of linkage disequilibrium (as measured by $r^2$) in the 1000 Genomes European reference panel between each SNP (circles) and the purple diamond SNP is indicated by the color scale at the top left. Larger values of $r^2$ indicate greater linkage disequilibrium. (A) The SNP with the highest p-value in *BMPR1B*, rs3406382, is labeled with a purple diamond. (B) The cluster of nine SNPs in high LD with the purple diamond SNP rs4397000, and in lower LD with rs3406382 (blue circle). SNP = single nucleotide polymorphism, PAE = prenatal alcohol exposure, LD = linkage disequilibrium.

**Figure 8. Mandible volume by rs4397000 genotype in BMPR1B and alcohol exposure.** Mandible volume in children of European and African ancestry recruited with and without alcohol exposure according to genotype. In EA individuals with the CC genotype, mandible volume was significantly decreased in alcohol exposed vs unexposed individuals. In alcohol exposed EA individuals mandible volume was decreased in those with the CC genotype compared to those with the AA/AC genotypes.

**Supplementary Figure Legends**

**Supplement Figure 1. Visual representation of the 20 landmark locations used to induce the dense surface correspondence.** (A-B) left and right endocanthion, exocanthion, tragion, otobasion inferius, crista philtrum, cheilion, and alare; nasion, pronasale, subnasale, labiale superius, labiale inferius, and gnathion. (B) The landmarks labiuminferius, gnathion, and otobasion inferior define the tetrahedron (1, 2,3, 4). The volume of the tetrahedron is calculated as (1/6)det (axayaz1; bxbybz1; cxcycz1; dxdydz1).

**Supplement Figure 2. A wide spectrum of viscerocranial malformations was observed in ethanol-treated *bmp4*$^{+/-}$*;smad5*$^{-/-}$ larva.** (A-C) Whole-mount images of viscerocranium at 5 dpf larva. Cartilage is blue and bone is red (Ventral views, anterior to the left, scale bar: 100 μm). (A-C) Ethanol exposure on *bmp4*$^{+/-}$*;smad5*$^{-/-}$ larva range from stereotypical *smad5* mutant phenotypes to severe ethanol-induced phenotypes to the viscerocranium (Supplemental Table 1).

**Supplement Figure 3. Ethanol exposure alters size of the anterior pharyngeal endoderm in *bmp4*$^{+/-}$*;smad5*$^{-/-}$ larva.** (A-F) Length and width measures of the anterior pharyngeal endoderm. (A-C) Ethanol exposure decreased endoderm length but not head length in *bmp4*$^{+/+}$*;smad5*$^{+/+}$ embryos but significantly increased endoderm length ethanol-treated *bmp4*$^{-/-}$*;smad5*$^{-/-}$ embryos. (D-F) Ethanol-treatment significantly increased in the ratio of endoderm width to head width in *bmp4*$^{-/-}$*;smad5*$^{-/-}$ embryos, though there was a trend in the increase in ethanol-treated *bmp4*$^{+/+}$*;smad5*$^{+/+}$ embryos as well, but not in head width (individual graph statistics in Supplemental Table 1).

# Figures

## Figure 1

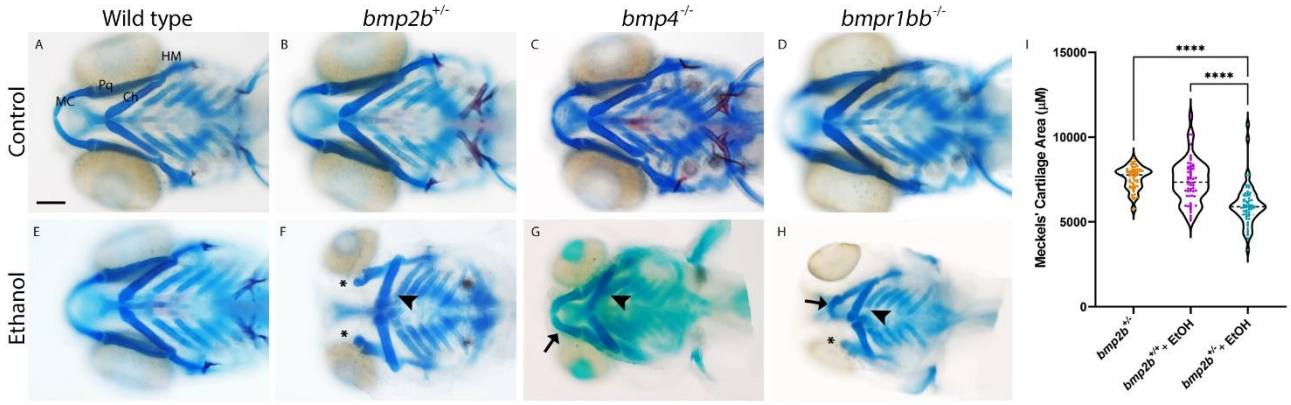

**Figure 2**

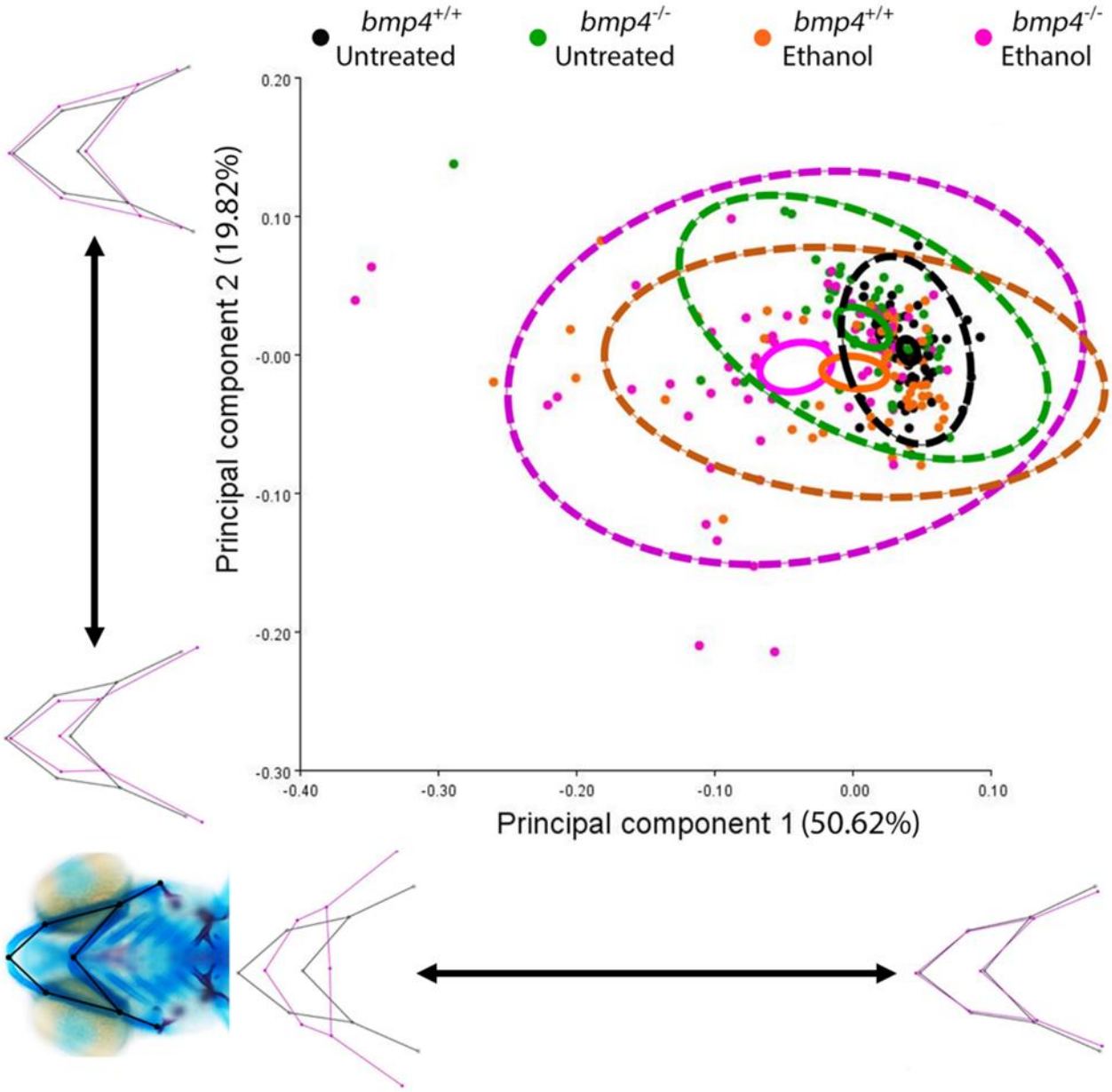
bmp4+/+ Untreated
bmp4-/- Untreated
bmp4+/+ Ethanol
bmp4-/- Ethanol
Principal component 2 (19.82%)
Principal component 1 (50.62%)
0.20
0.10
-0.00
-0.10
-0.20
-0.30
-0.40
-0.30
-0.20
-0.10
0.00
0.10

**Figure 3**

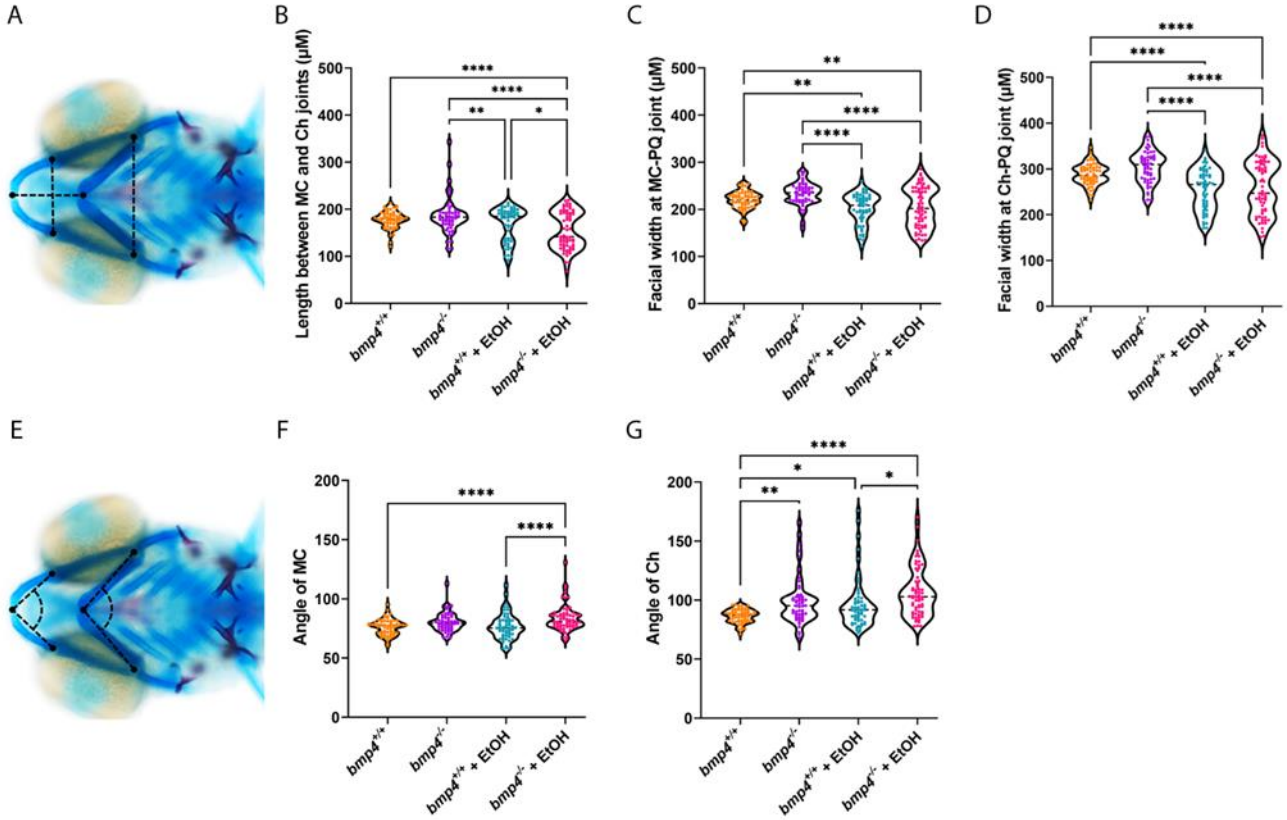
A
B
Length between MC and Ch joints (μM)
C
Facial width at MC-PQ joint (μM)
D
Facial width at Ch-PQ joint (μM)
E
F
Angle of MC
G
Angle of Ch
bmp4+/+
bmp4-/-
bmp4+/+ + EtOH
bmp4-/- + EtOH

**Figure 4**

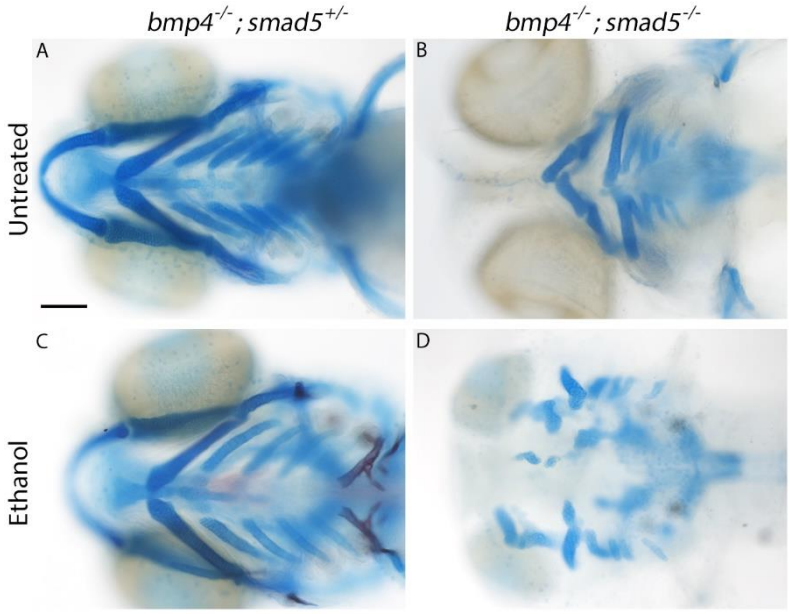

**Figure 5**

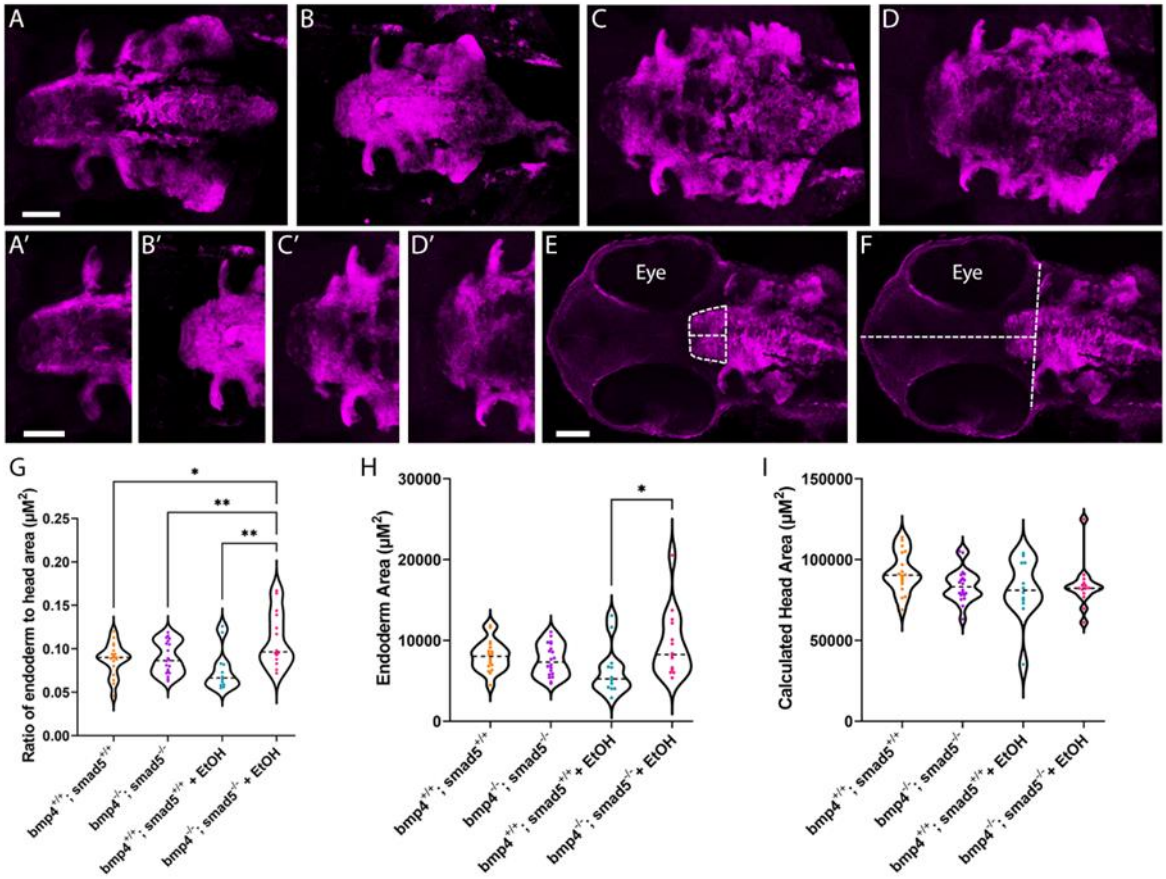
A
B
C
D
A′
B′
C′
D′
E
Eye
F
Eye
G
Ratio of endoderm to head area (μM²)
0.25
0.20
0.15
0.10
0.05
0.00
*
**
**
bmp4+/+; smad5+/+
bmp4-/-; smad5-/-
bmp4+/+; smad5+/+ + EtOH
bmp4-/-; smad5-/- + EtOH
H
Endoderm Area (μM²)
30000
20000
10000
0
*
bmp4+/+; smad5+/+
bmp4-/-; smad5-/-
bmp4+/+; smad5+/+ + EtOH
bmp4-/-; smad5-/- + EtOH
I
Calculated Head Area (μM²)
150000
100000
50000
0
bmp4+/+; smad5+/+
bmp4-/-; smad5-/-
bmp4+/+; smad5+/+ + EtOH
bmp4-/-; smad5-/- + EtOH

**Figure 6**

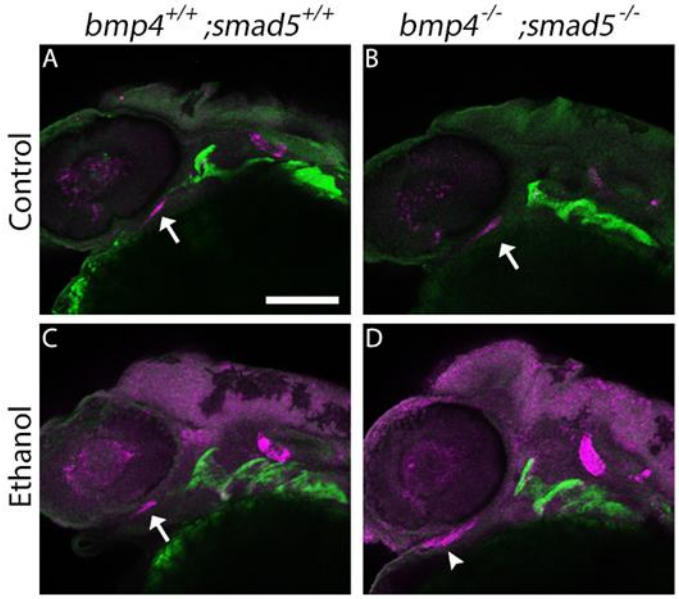

**Figure 7**

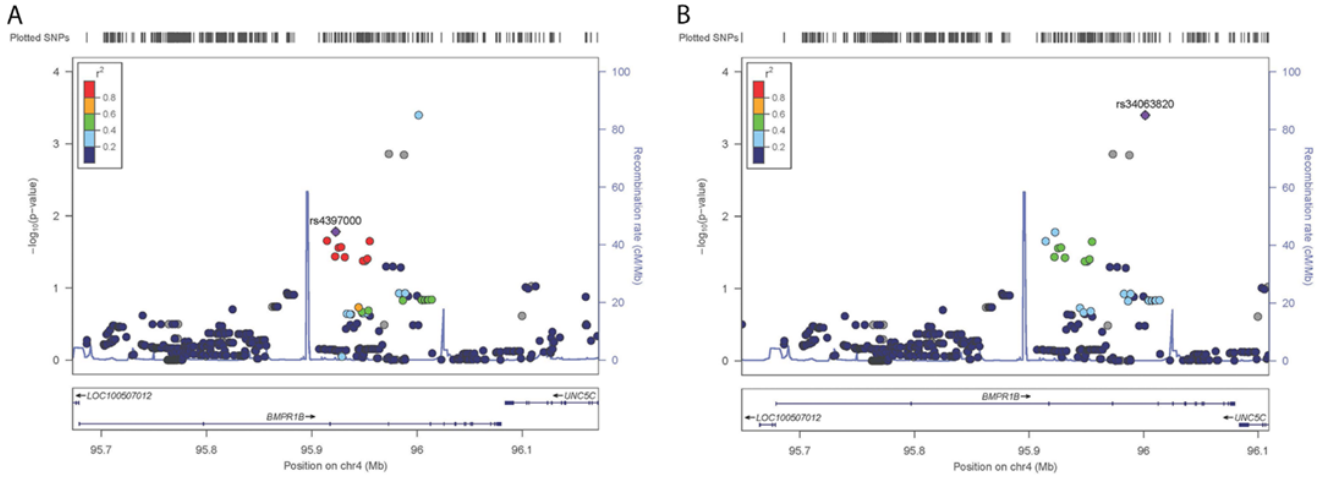
A
Plotted SNPs
rs4397000
LOC100507012
UNC5C
BMPR1B
Position on chr4 (Mb)
Recombination rate (cM/Mb)
B
Plotted SNPs
rs34063820
BMPR1B
LOC100507012
UNC5C
Position on chr4 (Mb)
Recombination rate (cM/Mb)

**Figure 8**

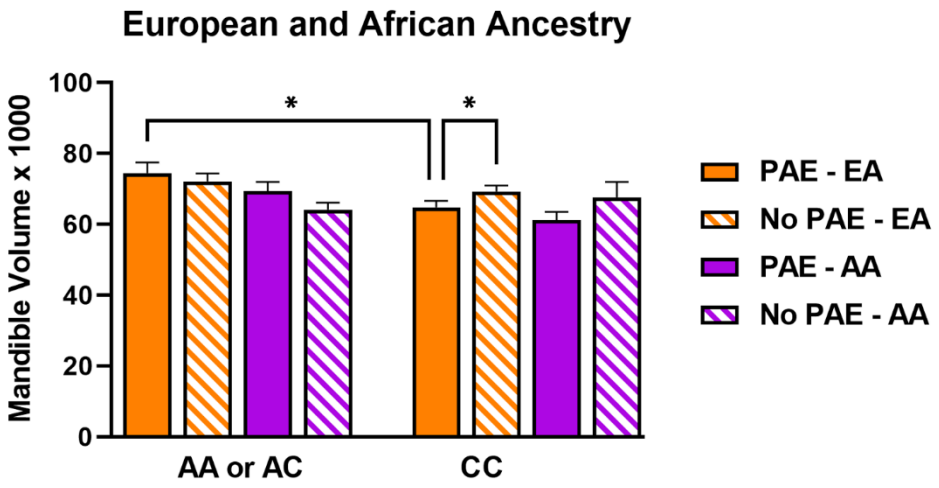
European and African Ancestry
Mandible Volume x 1000
100
80
60
40
20
0
*
*
AA or AC
CC
PAE - EA
No PAE - EA
PAE - AA
No PAE - AA

**Table 1**

| Table 1 | | | | | | |
|---|---|---|---|---|---|---|
| **Experiments** | **Untreated Embryos** | **EtOH-treated Embryos** | **Jaw Malformations** | **Percent** | **Jaw Loss** | **Percent** |
| | | | ***bmp2b*** | | | |
| 1 | 37 | 41 | 6 | 14.6% | 0 | 0.0% |
| 2 | 45 | 41 | 10 | 24.4% | 3 | 7.3% |
| 3 | 37 | 115 | 20 | 17.4% | 4 | 3.5% |
| 4 | 80 | 46 | 9 | 19.6% | 5 | 10.9% |
| 5 | 64 | 61 | 12 | 19.7% | 1 | 1.6% |
| 6 | 75 | 193 | 26 | 13.5% | 7 | 3.6% |
| 7 | 23 | 24 | 0 | 0.0% | 4 | 16.7% |
| Totals | 361 | 521 | 83 | 15.9% | 24 | 4.6% |
| | | | ***bmp4*** | | | |
| 1 | 24 | 63 | 30 | 47.6% | 3 | 4.8% |
| 2 | 41 | 131 | 38 | 29.0% | 2 | 1.5% |
| 3 | 42 | 38 | 24 | 63.2% | 2 | 5.3% |
| 4 | 51 | 94 | 20 | 21.3% | 16 | 17.0% |
| 5 | 44 | 82 | 42 | 51.2% | 2 | 2.4% |
| Totals | 202 | 408 | 154 | 37.7% | 25 | 6.1% |
| | | | ***bmpr1bb*** | | | |
| 1 | 105 | 82 | 41 | 50.0% | 1 | 1.2% |
| 2 | 48 | 38 | 1 | 2.6% | 0 | 0.0% |
| 3 | 154 | 69 | 13 | 18.8% | 4 | 5.8% |
| Totals | 307 | 189 | 55 | 29.1% | 5 | 2.6% |

**Table 2**

| Length at MC-Ch joints | | |
|---|---|---|
| **ANOVA** | F = 14.94 | P < 0.0001 |
| **Tukey's Comparisons** | | |
| *bmp4* $^{+/+}$ vs *bmp4* $^{-/-}$ | p = 0.3411 | |
| *bmp4* $^{+/+}$ vs *bmp4* $^{+/+}$ + EtOH | p = 0.3296 | |
| *bmp4* $^{+/+}$ vs *bmp4* $^{-/-}$ + EtOH | p < 0.0001 | |
| *bmp4* $^{-/-}$ vs *bmp4* $^{+/+}$ + EtOH | p = 0.006 | |
| *bmp4* $^{-/-}$ vs *bmp4* $^{-/-}$ + EtOH | p < 0.0001 | |
| *bmp4* $^{+/+}$ + EtOH vs *bmp4* $^{-/-}$ + EtOH | p = 0.0144 | |

| Width at MC/PQ joint | | |
|---|---|---|
| **ANOVA** | F = 15.62 | P < 0.0001 |
| **Tukey's Comparisons** | | |
| *bmp4* $^{+/+}$ vs *bmp4* $^{-/-}$ | p = 0.0508 | |
| *bmp4* $^{+/+}$ vs *bmp4* $^{+/+}$ + EtOH | p = 0.0055 | |
| *bmp4* $^{+/+}$ vs *bmp4* $^{-/-}$ + EtOH | p = 0.0082 | |
| *bmp4* $^{-/-}$ vs *bmp4* $^{+/+}$ + EtOH | p < 0.0001 | |
| *bmp4* $^{-/-}$ vs *bmp4* $^{-/-}$ + EtOH | p < 0.0001 | |
| *bmp4* $^{+/+}$ + EtOH vs *bmp4* $^{-/-}$ + EtOH | p = 0.997 | |

| Width at Ch-PQ joint | | |
|---|---|---|
| **ANOVA** | F = 23.77 | P < 0.0001 |
| **Tukey's Comparisons** | | |
| *bmp4* $^{+/+}$ vs *bmp4* $^{-/-}$ | p = 0.0858 | |
| *bmp4* $^{+/+}$ vs *bmp4* $^{+/+}$ + EtOH | p < 0.0001 | |
| *bmp4* $^{+/+}$ vs *bmp4* $^{-/-}$ + EtOH | p < 0.0002 | |
| *bmp4* $^{-/-}$ vs *bmp4* $^{+/+}$ + EtOH | p < 0.0003 | |
| *bmp4* $^{-/-}$ vs *bmp4* $^{-/-}$ + EtOH | p < 0.0004 | |
| *bmp4* $^{+/+}$ + EtOH vs *bmp4* $^{-/-}$ + EtOH | p = 0.9993 | |

| Angle at MC | | |
|---|---|---|
| **ANOVA** | F = 10.01 | P < 0.0001 |
| **Tukey's Comparisons** | | |
| *bmp4* $^{+/+}$ vs *bmp4* $^{-/-}$ | p = 0.0653 | |
| *bmp4* $^{+/+}$ vs *bmp4* $^{+/+}$ + EtOH | p = 0.9995 | |
| *bmp4* $^{+/+}$ vs *bmp4* $^{-/-}$ + EtOH | p < 0.0001 | |
| *bmp4* $^{-/-}$ vs *bmp4* $^{+/+}$ + EtOH | p = 0.0866 | |
| *bmp4* $^{-/-}$ vs *bmp4* $^{-/-}$ + EtOH | p = 0.1873 | |
| *bmp4* $^{+/+}$ + EtOH vs *bmp4* $^{-/-}$ + EtOH | p < 0.0001 | |

| Angle at Ch | | |
|---|---|---|
| **ANOVA** | F = 12.33 | P < 0.0001 |
| **Tukey's Comparisons** | | |
| *bmp4* $^{+/+}$ vs *bmp4* $^{-/-}$ | p = 0.0015 | |
| *bmp4* $^{+/+}$ vs *bmp4* $^{+/+}$ + EtOH | p = 0.0192 | |
| *bmp4* $^{+/+}$ vs *bmp4* $^{-/-}$ + EtOH | p < 0.0001 | |
| *bmp4* $^{-/-}$ vs *bmp4* $^{+/+}$ + EtOH | p = 0.8338 | |
| *bmp4* $^{-/-}$ vs *bmp4* $^{-/-}$ + EtOH | p = 0.1914 | |
| *bmp4* $^{+/+}$ + EtOH vs *bmp4* $^{-/-}$ + EtOH | p = 0.0204 | |

**Table 3**

| Ratio of Endoderm to Head Area | | | Endoderm Area | | | Head Area (Calculated) | | |
|---|---|---|---|---|---|---|---|---|
| **ANOVA** | F = 5.919 | P = 0.0019 | **ANOVA** | F = 2.801 | P = 0.0518 | **ANOVA** | F = 1.958 | P = 0.1353 |
| **Tukey's Comparisons** | | | **Tukey's Comparisons** | | | **Tukey's Comparisons** | | |
| *bmp4* $^{+/+}$;smad5$^{+/+}$ vs *bmp4* $^{-/-}$*;smad5* $^{+/+}$ | p = 0.9989 | | *bmp4* $^{+/+}$;smad5$^{+/+}$ vs *bmp4* $^{-/-}$*;smad5* $^{+/+}$ | p = 0.8751 | | *bmp4* $^{+/+}$;smad5$^{+/+}$ vs *bmp4* $^{-/-}$*;smad5* $^{+/+}$ | p = 0.3505 | |
| *bmp4* $^{+/+}$;smad5$^{+/+}$ vs *bmp4* $^{+/+-}$*;smad5* $^{+/+}$ + EtOH | p = 0.8727 | | *bmp4* $^{+/+}$;smad5$^{+/+}$ vs *bmp4* $^{+/+-}$*;smad5* $^{+/+}$ + EtOH | p = 0.8751 | | *bmp4* $^{+/+}$;smad5$^{+/+}$ vs *bmp4* $^{+/+-}$*;smad5* $^{+/+}$ + EtOH | p = 0.1492 | |
| *bmp4* $^{+/+}$;smad5$^{+/+}$ vs *bmp4* $^{-/-}$*;smad5* $^{-/-}$ + EtOH | p = 0.0127 | | *bmp4* $^{+/+}$;smad5$^{+/+}$ vs *bmp4* $^{-/-}$*;smad5* $^{-/-}$ + EtOH | p = 0.8751 | | *bmp4* $^{+/+}$;smad5$^{+/+}$ vs *bmp4* $^{-/-}$*;smad5* $^{-/-}$ + EtOH | p = 0.2876 | |
| *bmp4* $^{-/-}$;smad5$^{-/-}$ vs *bmp4* $^{+/+}$*;smad5* $^{+/+}$ + EtOH | p = 0.9211 | | *bmp4* $^{-/-}$;smad5$^{-/-}$ vs *bmp4* $^{+/+}$*;smad5* $^{+/+}$ + EtOH | p = 0.8751 | | *bmp4* $^{-/-}$;smad5$^{-/-}$ vs *bmp4* $^{+/+}$*;smad5* $^{+/+}$ + EtOH | p = 0.8835 | |
| *bmp4* $^{-/-}$;smad5$^{-/-}$ vs *bmp4* $^{-/-}$*;smad5* $^{-/-}$ + EtOH | p = 0.0089 | | *bmp4* $^{-/-}$;smad5$^{-/-}$ vs *bmp4* $^{-/-}$*;smad5* $^{-/-}$ + EtOH | p = 0.1277 | | *bmp4* $^{-/-}$;smad5$^{-/-}$ vs *bmp4* $^{-/-}$*;smad5* $^{-/-}$ + EtOH | p = 0.992 | |
| *bmp4* $^{-/-}$;smad5$^{-/-}$ + EtOH vs *bmp4* $^{-/-}$*;smad5* $^{-/-}$ + EtOH | p = 0.0033 | | *bmp4* $^{-/-}$;smad5$^{-/-}$ + EtOH vs *bmp4* $^{-/-}$*;smad5* $^{-/-}$ + EtOH | p = 0.0494 | | *bmp4* $^{-/-}$;smad5$^{-/-}$ + EtOH vs *bmp4* $^{-/-}$*;smad5* $^{-/-}$ + EtOH | p = 0.9686 | |

**Supplemental Figure 1**

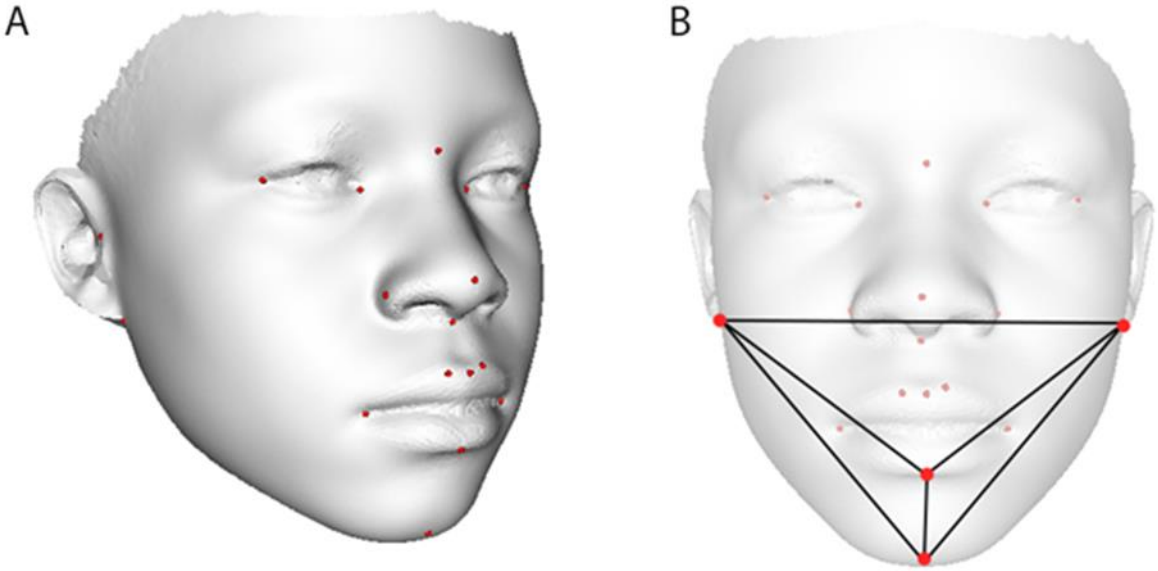

**Supplemental Figure 2**

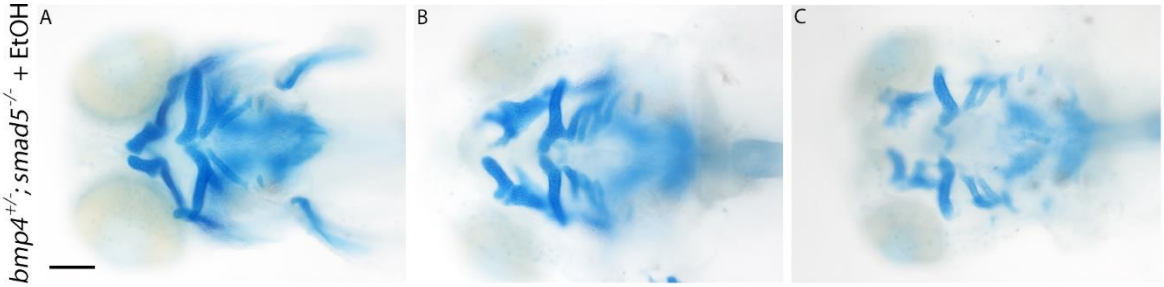

**Supplemental Figure 3**

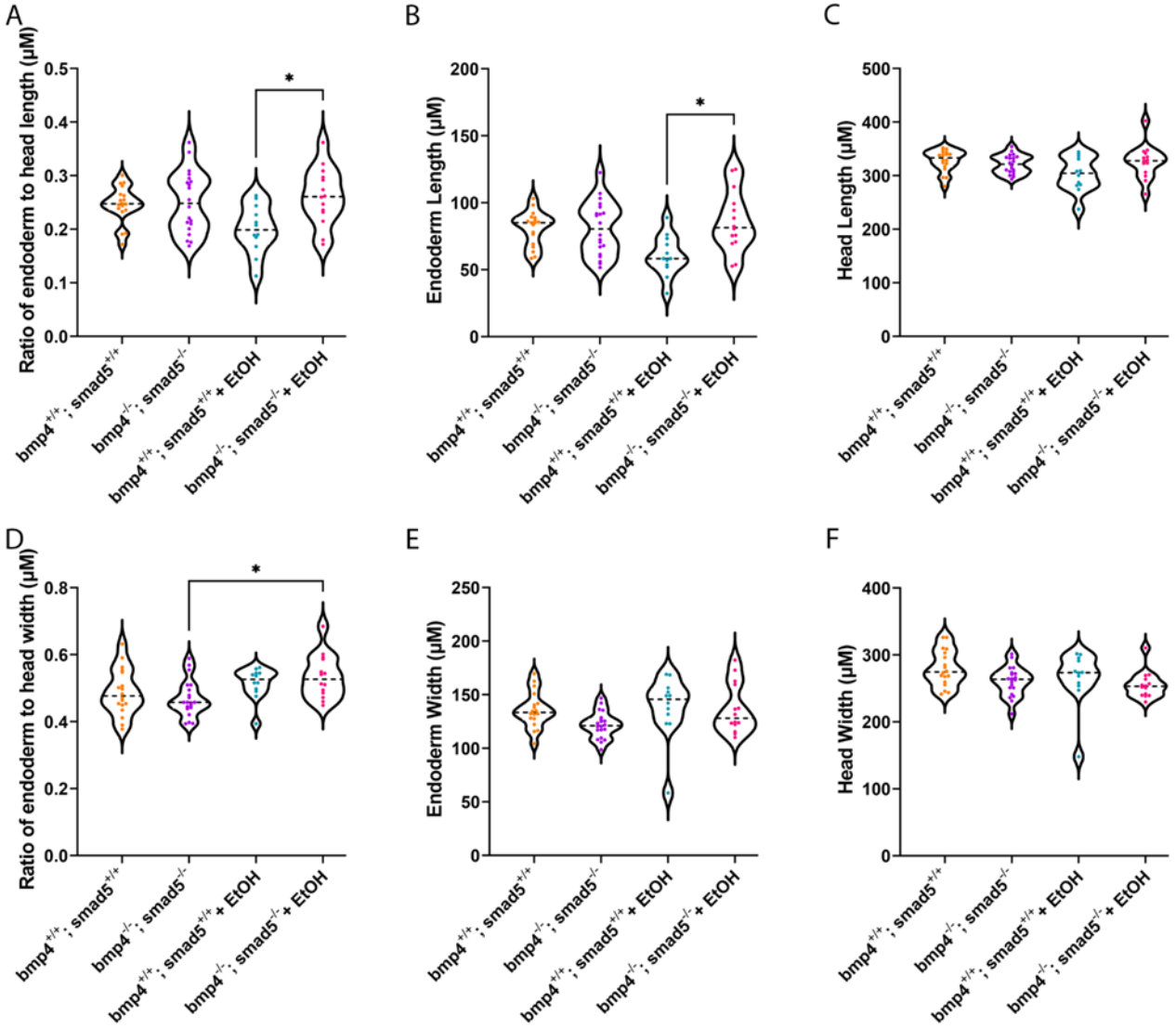

**Supplemental Table 1**

| Ratio of Endoderm to Head Length | | |
|---|---|---|
| **ANOVA** | F = 2.930 | P = 0.0448 |
| **Tukey's Comparisons** | | |
| *bmp4* $^{+/+}$;smad5$^{+/+}$ vs *bmp4* $^{-/-}$*;smad5* $^{+/+}$ | p = 0.9989 | |
| *bmp4* $^{+/+}$;smad5$^{+/+}$ vs *bmp4* $^{+/+-}$*;smad5* $^{+/+}$ + EtOH | p = 0.8727 | |
| *bmp4* $^{+/+}$;smad5$^{+/+}$ vs *bmp4* $^{-/-}$*;smad5* $^{-/-}$ + EtOH | p = 0.0127 | |
| *bmp4* $^{-/-}$;smad5$^{-/-}$ vs *bmp4* $^{+/+}$*;smad5* $^{+/+}$ + EtOH | p = 0.9211 | |
| *bmp4* $^{-/-}$;smad5$^{-/-}$ vs *bmp4* $^{-/-}$*;smad5* $^{-/-}$ + EtOH | p = 0.0089 | |
| *bmp4* $^{-/-}$;smad5$^{-/-}$ + EtOH vs *bmp4* $^{-/-}$*;smad5* $^{-/-}$ + EtOH | p = 0.0033 | |

| Endoderm Length | | |
|---|---|---|
| **ANOVA** | F = 3.811 | P = 0.0169 |
| **Tukey's Comparisons** | | |
| *bmp4* $^{+/+}$;smad5$^{+/+}$ vs *bmp4* $^{-/-}$*;smad5* $^{+/+}$ | p = 0.8751 | |
| *bmp4* $^{+/+}$;smad5$^{+/+}$ vs *bmp4* $^{+/+-}$*;smad5* $^{+/+}$ + EtOH | p = 0.8751 | |
| *bmp4* $^{+/+}$;smad5$^{+/+}$ vs *bmp4* $^{-/-}$*;smad5* $^{-/-}$ + EtOH | p = 0.8751 | |
| *bmp4* $^{-/-}$;smad5$^{-/-}$ vs *bmp4* $^{+/+}$*;smad5* $^{+/+}$ + EtOH | p = 0.8751 | |
| *bmp4* $^{-/-}$;smad5$^{-/-}$ vs *bmp4* $^{-/-}$*;smad5* $^{-/-}$ + EtOH | p = 0.1277 | |
| *bmp4* $^{-/-}$;smad5$^{-/-}$ + EtOH vs *bmp4* $^{-/-}$*;smad5* $^{-/-}$ + EtOH | p = 0.0494 | |

| Head Length | | |
|---|---|---|
| **ANOVA** | F = 2.309 | P = 0.0906 |
| **Tukey's Comparisons** | | |
| *bmp4* $^{+/+}$;smad5$^{+/+}$ vs *bmp4* $^{-/-}$*;smad5* $^{+/+}$ | p = 0.3505 | |
| *bmp4* $^{+/+}$;smad5$^{+/+}$ vs *bmp4* $^{+/+-}$*;smad5* $^{+/+}$ + EtOH | p = 0.1492 | |
| *bmp4* $^{+/+}$;smad5$^{+/+}$ vs *bmp4* $^{-/-}$*;smad5* $^{-/-}$ + EtOH | p = 0.2876 | |
| *bmp4* $^{-/-}$;smad5$^{-/-}$ vs *bmp4* $^{+/+}$*;smad5* $^{+/+}$ + EtOH | p = 0.8835 | |
| *bmp4* $^{-/-}$;smad5$^{-/-}$ vs *bmp4* $^{-/-}$*;smad5* $^{-/-}$ + EtOH | p = 0.992 | |
| *bmp4* $^{-/-}$;smad5$^{-/-}$ + EtOH vs *bmp4* $^{-/-}$*;smad5* $^{-/-}$ + EtOH | p = 0.9686 | |

| Ratio of Endoderm to Head Width | | |
|---|---|---|
| **ANOVA** | F = 3.063 | P = 0.0386 |
| **Tukey's Comparisons** | | |
| *bmp4* $^{+/+}$;smad5$^{+/+}$ vs *bmp4* $^{-/-}$*;smad5* $^{+/+}$ | p = 0.8133 | |
| *bmp4* $^{+/+}$;smad5$^{+/+}$ vs *bmp4* $^{+/+-}$*;smad5* $^{+/+}$ + EtOH | p = 0.652 | |
| *bmp4* $^{+/+}$;smad5$^{+/+}$ vs *bmp4* $^{-/-}$*;smad5* $^{-/-}$ + EtOH | p = 0.1846 | |

| Endoderm Width | | |
|---|---|---|
| **ANOVA** | F = 1.869 | P = 0.1499 |
| **Tukey's Comparisons** | | |
| *bmp4* $^{+/+}$;smad5$^{+/+}$ vs *bmp4* $^{-/-}$*;smad5* $^{+/+}$ | p = 0.2316 | |
| *bmp4* $^{+/+}$;smad5$^{+/+}$ vs *bmp4* $^{+/+-}$*;smad5* $^{+/+}$ + EtOH | p = 0.9983 | |
| *bmp4* $^{+/+}$;smad5$^{+/+}$ vs *bmp4* $^{-/-}$*;smad5* $^{-/-}$ + EtOH | p = 0.9993 | |

| Head Width | | |
|---|---|---|
| **ANOVA** | F = 2.691 | P = 0.0587 |
| **Tukey's Comparisons** | | |
| *bmp4* $^{+/+}$;smad5$^{+/+}$ vs *bmp4* $^{-/-}$*;smad5* $^{+/+}$ | p = 0.1886 | |
| *bmp4* $^{+/+}$;smad5$^{+/+}$ vs *bmp4* $^{+/+-}$*;smad5* $^{+/+}$ + EtOH | p = 0.3263 | |
| *bmp4* $^{+/+}$;smad5$^{+/+}$ vs *bmp4* $^{-/-}$*;smad5* $^{-/-}$ + EtOH | p = 0.0523 | |

| | | | | | |
|---|---|---|---|---|---|
| *bmp4* $^{-/-}$;smad5$^{-/-}$ vs *bmp4* $^{+/+}$*;smad5* $^{+/+}$ + EtOH | p = 0.2343 | *bmp4* $^{-/-}$;smad5$^{-/-}$ vs *bmp4* $^{+/+}$*;smad5* $^{+/+}$ + EtOH | p = 0.277 | *bmp4* $^{-/-}$;smad5$^{-/-}$ vs *bmp4* $^{+/+}$*;smad5* $^{+/+}$ + EtOH | p > 0.9999 |
| *bmp4* $^{-/-}$;smad5$^{-/-}$ vs *bmp4* $^{-/-}$*;smad5* $^{-/-}$ + EtOH | p = 0.0324 | *bmp4* $^{-/-}$;smad5$^{-/-}$ vs *bmp4* $^{-/-}$*;smad5* $^{-/-}$ + EtOH | p = 0.2553 | *bmp4* $^{-/-}$;smad5$^{-/-}$ vs *bmp4* $^{-/-}$*;smad5* $^{-/-}$ + EtOH | p = 0.8529 |
| *bmp4* $^{-/-}$;smad5$^{-/-}$ + EtOH vs *bmp4* $^{-/-}$*;smad5* $^{-/-}$ + EtOH | p = 0.8716 | *bmp4* $^{-/-}$;smad5$^{-/-}$ + EtOH vs *bmp4* $^{-/-}$*;smad5* $^{-/-}$ + EtOH | p > 0.9999 | *bmp4* $^{-/-}$;smad5$^{-/-}$ + EtOH vs *bmp4* $^{-/-}$*;smad5* $^{-/-}$ + EtOH | p = 0.866 |